JGR Solid Earth

Extent and Cessation of the Mid-Cretaceous Hikurangi Plateau Underthrusting: Impact on Global Plate Tectonics and the Submarine Chatham Rise

Florian Riefstahl[1] , **Karsten Gohl[1]** , **Bryan Davy[2]** , and **Rachel Barrett[3]**

[1]Alfred Wegener Institute Helmholtz-Centre for Polar and Marine Research, Bremerhaven, Germany, [2]GNS Science, Lower Hutt, New Zealand, [3]Institut für Geowissenschaften, Christian-Albrechts-Universität zu Kiel, Kiel, Germany

Abstract Subduction of oceanic plateaux are events that have occurred infrequently in Earth's history. Although rare, these events are thought to considerably influence regional tectonics and global plate motions. In the mid-Cretaceous the oceanic Hikurangi Plateau collided with the formerly active East Gondwana margin: An event which falls into the same of a sudden change from subduction to extensional processes, including graben formation, development rift basin development, and exhumation of metamorphic core complexes in the Zealandia continent as well as a global-scale plate reorganization event. In this study, we use recently acquired seismic refraction and gravity data along one profile across the submarine Chatham Rise, which represent a former accretionary wedge of the East Gondwana subduction zone. We demonstrate that the southward extent of the subducted Hikurangi Plateau in the lower crust beneath the submarine Chatham Rise along our profile is only ~150. This is ~150 km less than the previously suggested extent. Furthermore, we interpret that a slice of the subducted Phoenix Plate remains attached to the southern edge of the Hikurangi Plateau. We suggest that cessation of subduction in response to the Hikurangi Plateau jamming as well as the rollback and detachment of the Phoenix Plate slab played an important role in the changing tectonic forces across Zealandia in mid-Cretaceous. Moreover, we suggest that the subduction cessation along the Hikurangi Plateau segment led to the fragmentation of the Gondwana subduction zone and Phoenix Plate, which significantly influenced and potentially prolonged the global mid-Cretaceous plate reorganization event.

1. Introduction

The formation of oceanic plateaux—extraordinarily thick oceanic crust primarily resulting from primarily basaltic magmatism—is considered to be the most extreme volcanic events on Earth. The life cycle of oceanic plateaux may include obduction and enlargement of landmasses, underplating through shallow flat subduction or subduction and recycling back into the Earth's mantle; all of which represent rare events in global geodynamics. Their influence on global plate tectonics and its significance within the Wilson cycle (Dewey & Burke, 1974) remain, however, enigmatic. Two well-studied, but contradictory, examples of the influence of oceanic plateaux on regional and global tectonics include (a) the still ongoing collision of the Ontong Java Plateau with the Melanesian arc, which led to partial subduction and crustal accretion (Mann & Taira, 2004; Taira et al., 2004) and (b) the Late Cretaceous lithospheric removal of a subducted oceanic plateau beneath western North America, which led to regional-scale surface rebound and, thereby, initiated the Laramide Orogeny in North America (Liu et al., 2010). Both examples were accompanied by complex collisional tectonics, but while subduction of the oceanic plateau beneath western North America resulted in spatially limited uplift, the collision of the Ontong Java Plateau triggered subduction cessation and reversal, which influenced the motion of the Australian Plate in the mid-Miocene (Knesel et al., 2008) and induced rapid changes in plate motions in the late Miocene (Austermann et al., 2011). Accordingly, oceanic plateau collision and subduction are capable of triggering both far-field and local tectonic effects.

Another unique example for the subduction of oceanic plateaux is the Hikurangi Plateau (Figure 1a), which has undergone a twofold subduction history. The southward-directed collision of the Hikurangi Plateau with the long-lived East Gondwana active margin during the mid-Cretaceous is believed to have initiated the end of subduction activity in the area of New Zealand's South Island and Chatham Rise (Davy et al., 2008;
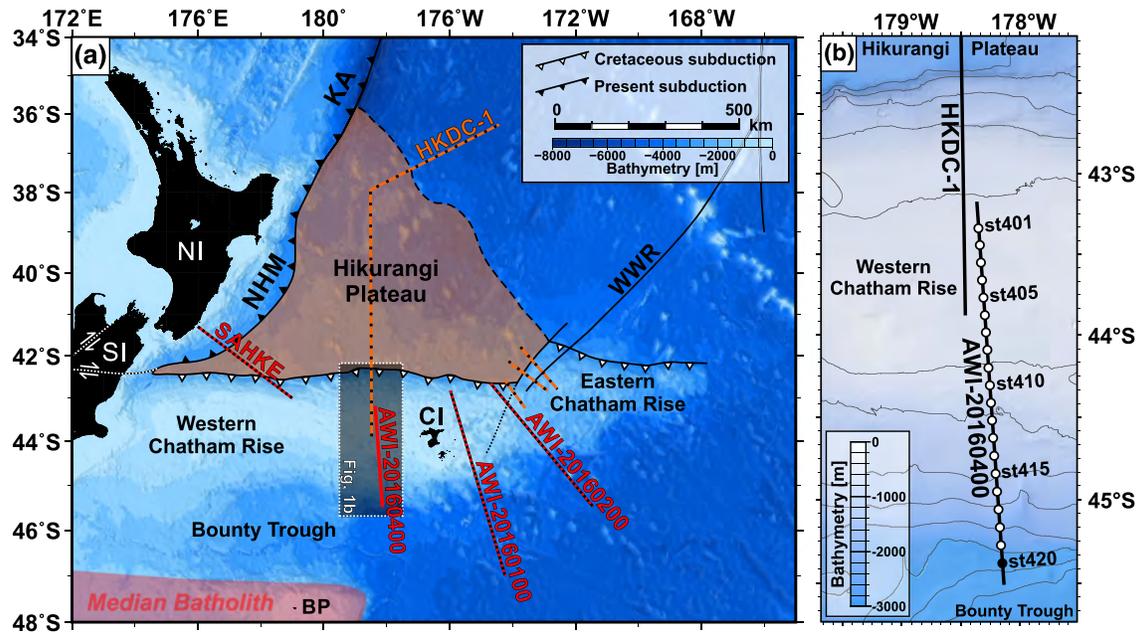
Figure 1. (a) Bathymetry map of the Chatham Rise and Hikurangi Plateau showing locations of seismic refraction profile AWI-20160400 (red, this study) and seismic profiles from previous studies (Barrett et al., 2018; Davy et al., 2008; Mochizuki et al., 2019; Riefstahl et al., 2020) that enabled thickness estimates of the Hikurangi Plateau in the area of Chatham Rise (seismic refraction profiles = red dotted lines; MCS reflection and gravity data = orange dotted lines). Several more MCS reflection lines and dense networks of MCS reflection lines are recorded in that area and are not shown (e.g., Barker et al., 2009; Bland et al., 2015). BP = bounty platform, CI = Chatham Islands, KA = Kermadec arc, NI = North Island, SI = South Island, WWR = West wishbone ridge. (b) Detailed map view of seismic refraction profile AWI-20160400 that is a southward extension of the previously collected seismic reflection profile HKDC-1. White dots mark locations of ocean-bottom seismometers/hydrophones (OBS/OBH). The black dot marks a failed OBS record (st420).

Figure 1a). Subsequently, extensional processes, including the formation of rift grabens and intraplate volcanic activity, started to affect the micro-continent "Zealandia." The collision of the Hikurangi Plateau with the East Gondwana margin, the end of compressional tectonics, and the initiation of extension all fell within the time range of a global-scale plate reorganization event that affected all major tectonic plates (Matthews et al., 2012). The second stage of subduction of the Hikurangi Plateau, this time directed westward at the Australian-Pacific plate boundary beneath the North Island of New Zealand, began at least in the Miocene and is still ongoing (Reyners, 2013; Timm et al., 2014).

In this study, we present seismic reflection and wide-angle reflection/refraction data along a profile across the southwestern Chatham Rise margin, where the Hikurangi Plateau is thought to have underthrust the former East Gondwana active margin. We combine our newly acquired data with published seismic reflection and wide-angle reflection/refraction data to map the extent of the underthrusted Hikurangi Plateau and oceanic crust of the former Phoenix Plate beneath the Chatham Rise. The aim of this is to shed light on the processes of oceanic plateau subduction, resulting regional effects, and global consequences on plate tectonics.

2. Geological and Tectonic Background

The Hikurangi Plateau (Figure 1a) formed between 125 and 120 Ma as part of the Ontong Java Nui superplateau, the Earth's largest oceanic plateau (Hoernle et al., 2010; Taylor, 2006). Shortly after its formation, Ontong Java Nui rifted and drifted apart into three major pieces: the Ontong Java, Manihiki, and Hikurangi plateaux (Hochmuth & Gohl, 2017; Hochmuth et al., 2015). The Hikurangi Plateau drifted southward before underthrusting, partially subducting beneath, and jamming a ~1,500 km-wide section of the East Gondwana subduction zone at ~100 Ma (Davy, 2014; Davy et al., 2008).

Present knowledge of the extent and thickness of the subducted and underthrusted Hikurangi Plateau beneath southern Zealandia, especially along the previously active Cretaceous margin (Figure 1a), is

based on limited data. The Hikurangi Plateau's eastern extent is coincident with a prominent mid-Cretaceous dextral strike-slip fault zone—the West Wishbone Ridge (WWR, Figure 1a), which evolved in response to plateau collision (Barrett et al., 2018). The top of the subducted Hikurangi Plateau has been imaged with seismic reflection profiles beneath several areas of the present-day submarine Chatham Rise and up to 100 km south of it (Figure 1a; Bland et al., 2015; Davy et al., 2008). The Chatham Rise itself mainly consists of Mesozoic graywackes and schists of variable metamorphic grade typical of an accretionary wedge (e.g., Mortimer et al., 2016, 2019). Gravity models suggest a thickness of 12–17 km for the southern Hikurangi Plateau north of Chatham Rise (Barrett et al., 2018; Davy et al., 2008). In the area where the western Hikurangi Plateau is currently subducting westward beneath the North Island, seismic refraction profiles indicate that the plateau is significantly thinner, reaching a thickness of only 10 km (Mochizuki et al., 2019; Scherwath et al., 2010). Further north along the southern Kermadec arc (Figure 1a), geochemical variations of arc basalts-andesites provide evidence that a much larger proportion of the northwestern Hikurangi Plateau has been subducted within the past 10 Myr (Timm et al., 2014, 2016). V_p and V_p/V_s models based on seismological data suggest a thickness of 30–35 km for the western Hikurangi Plateau in the area beneath the lower North Island and South Island, where it is already deeply subducted to depths of 65–100 km (Reyners et al., 2011, 2017). On the basis of these models, Reyners et al. (2011) inferred that the entire Chatham Rise is "underplated" by the Hikurangi Plateau. Detailed analyses of gravity gradient fabrics led Davy (2014) to extend the limit of the Hikurangi Plateau southward, beneath the inner Bounty Trough. However, the full southern extent of the Hikurangi Plateau remains poorly constrained. Seismic refraction and deep-crustal seismic reflection studies indicate the presence of old oceanic crust of normal thickness beneath the sedimentary basins and stretched continental crust off the east coast of the South Island (Godfrey et al., 2001; Mortimer et al., 2002; Scherwath et al., 2003; Van Avendonk et al., 2004), highlighting the absence of the Hikurangi Plateau in this region.

Shortly after subduction cessation and jamming of the Hikurangi Plateau, the East Gondwana margin was affected by widespread extension and rifting during the "Zealandia Rift Phase." Different hypothesis exist to explain this rapid change in the tectonic regime: Bradshaw (1989) and Luyendyk et al. (2001) suggest that a spreading ridge sub-parallel was subducted, whereas Davy (2014) suggests that dextral strike-slip motions along the WWR transferred extension into Gondwana's interior. Evidence for this event is provided by a major Albian unconformity that has been radiometrically dated at ~100 Ma with the youngest associated zircon population (Laird & Bradshaw, 2004). This rapid transition between tectonic regimes is also made evident by a switch from arc-constructive processes and subduction-related magmatism in the Median Batholith (Figure 1a), to arc-destructive processes such as detachment faulting and metamorphic doming (Schwartz et al., 2016). Long-lasting arc magmatism was replaced by alkaline intraplate magmatism, which was spatially widespread but overall of low volume (Hoernle et al., 2020; McCoy-West et al., 2010; Mortimer et al., 2016; Panter et al., 2006; Tulloch et al., 2019; van der Meer et al., 2016, 2017). Crustal extension in the form of half-graben formation was substantial and affected the forearc and back-arc of the Median Batholith (Tulloch et al., 2019), as well as terrestrial sediments that had accumulated in several fault-controlled basins around the present North and South Islands in the mid-Cretaceous (e.g., Strogen et al., 2017). Opening of the Bounty Trough (Figure 1a) presumably also occurred during the "Zealandia Rift Phase" before seafloor spreading was initiated shortly after 90 Ma and the then-young Pacific-Antarctic Ridge separated Zealandia from Antarctica at ~80 Ma (Riefstahl et al., 2020).

3. Methods

3.1. Geophysical Data Acquisition and Data Processing

Deep-crustal wide-angle seismic reflection/refraction, multi-channel seismic (MCS), and gravity data were collected in 2016 along the N-S oriented profile AWI-20160400 (Figure 1b). The geophysical data were acquired during the SO246 expedition on RV Sonne in 2016 (Gohl & Werner, 2016). Twenty ocean-bottom seismometer (OBS) and hydrophone (OBH) systems were deployed at ~15 km spacings along the profile (Figure 1b), which extends across the southern Chatham Rise and northern margin of the Bounty Trough. Our profile extends the MCS profile HKDC-1 southward, where the top of the underthrust Hikurangi Plateau has been imaged up to 100 km south of the Chatham Rise accretionary wedge (Davy et al., 2008). Our seismic source comprised eight G-Guns in 2×4 G-Gun clusters with a total volume of 68 l (4,150 in.[3]) was fired at 205 bar every 60 s while towed 10 m below sea level. MCS reflection data

were recorded using the same shots for seismic refraction profiling and a 3,000 m long digital solid streamer with 240 channels (Sercel Sentinel™). All OBS/OBH instruments were recovered, but no data were recorded at station st420 due to malfunction (Figure 1b). Overall, the data quality is good to excellent, and the hydrophone channels provided the best data quality throughout. Furthermore, gravity data along profile AWI-20160400 were recorded by a LaCoste & Romberg S80/Ultrasys marine gravity meter.

The MCS data processing and modeling approach for the seismic refraction data and gravity follows Riefstahl et al. (2020). Processing steps for the MCS reflection data included common depth point (CDP) sorting, velocity-time profile analyses every 2.5 km (every 50th CDP on average), normal moveout corrections, stacking, and time migration (Figure 2). A 5/15–150/200 Hz trapezoidal bandpass filter was applied for displaying the time-migrated section. We relocated the OBS/OBH positions using the direct-wave arrivals. For interpretation and picking of the different reflection and refraction phase arrivals, we applied a 4–14 Hz bandpass filter and a 1,000 ms length automatic gain control with the software ZP (Zelt, 2004). Calculated individual picking uncertainties range between 25 and 200 ms depending on the signal-to-noise ratio.

3.2. P-Wave Velocity and Gravity Modeling Approach

P-wave velocity modeling was performed with the program Rayinvr (Zelt & Smith, 1992) and the graphical user interface PRay (Fromm, 2016) by using a top-to-bottom approach. As a priori information the multibeam bathymetry data along the profile were used to define the depth of the seafloor. Sedimentary cover and the basement structure of the Chatham Rise were incorporated from the MSC reflection data. We picked wide-angle reflection phases to help to determine the layer boundaries of the model. P-wave velocities for each layer were determined primarily from the refracted phases and subsequently refined to match all picks within their uncertainty range.

After the first top-to-down P-wave modeling iteration, we used the shipborne gravity data to model the density-depth distribution, which particularly helped to image zones that are sparsely resolved by refracted and reflected wave phases. For gravity modeling we setup a 2.5-D density model using the IGMAS+ software package (Schmidt et al., 2007) with the geometry and layer boundaries that were extracted from the P-wave velocity model. We subdivided layers only in the case of distinct lateral P-wave velocity variations. For the initial gravity model, average P-wave velocities for the resulting polygons were converted to densities using the P-wave velocity-density relationships of Barton (1986) and Christensen and Mooney (1995). We tried to fit the modeled free-air anomaly and the observed gravity data within a 5 mGal uncertainty range and took care that the modeled densities were not out of the uncertainties for the P-wave velocity-density relationships. After gravity modeling, we refined the P-wave velocity model and, thereafter, again the gravity model. After four cycles, the resulting P-wave velocity and gravity models (Figure 3) consistently explain the wave phase arrivals and gravity anomaly.

3.3. Uncertainty Estimation of the P-Wave Velocity Model

We estimated relative depth and velocity uncertainties of the P-wave velocity model according to Schlindwein and Jokat (1999). For this, we systematically perturbed model velocity and boundary knots until the calculated travel times were out of range of the assigned uncertainties of the observed data. These perturbations were performed layer-wise and individually for velocities and depths. The estimated relative uncertainties are listed in Table 1. Ray coverage and resolution plots are shown in Figures 4 and S1 in the Supporting Information. The inversion results corresponding to the presented P-wave velocity model (Figure 2a) are listed in Tables S1 and S2.

4. Modeling Results

In contrast with the area close to the Chatham Islands (e.g., Riefstahl et al., 2020; Wood et al., 1989; Wood & Anderson, 1989), the basement of the Chatham Rise along AWI-20160400 is completely covered with sedimentary strata. Along AWI-20160400, we find a series of 10–15 km broad half-grabens that are separated by several near-seafloor basement highs between 0 to 130 km along profile (Figures 2a and 3). The two largest and deepest graben structures are separated by two distinct basement highs at the southern slope of the Chatham Rise, where the seafloor deepens from ~400 to 3,500 m.b.s.l. (Figure 2). Further south of the basement high at ~200 km along profile, the upper surface of the basement is comparatively smooth, but some smaller half-graben structures are evident from the OBS and MCS data (Figures 2 and 3).
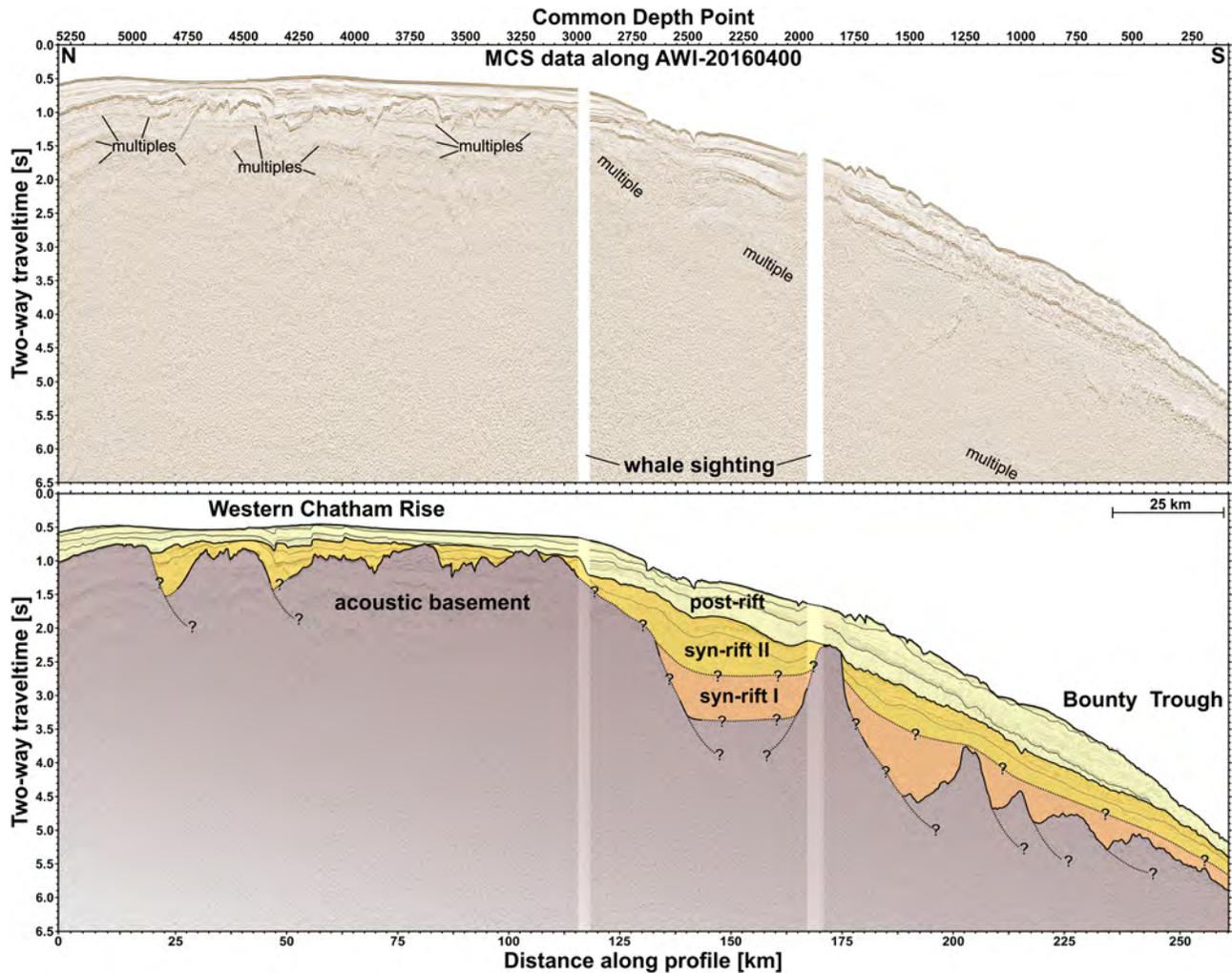
Figure 2. MCS reflection data and interpretation along seismic refraction profile AWI-20160400. The boundaries between syn-rift I and syn-rift II units are inferred from the OBS/OBH data.

Based on MCS data (Figure 2) and recorded wide-angle reflection/refraction phases (Figures 4a and 4b), we subdivide the sedimentary strata into (i) uppermost, well-layered sediments (layer sed1) that represent a post-rift deposit covering the Chatham Rise basement and underlying strata and (ii) syn-rift units (layers sed2 and sed3) that fill and cover the graben and half-graben structures. Layers sed2 and sed3 merge into a single layer along the top of the Chatham Rise (Figure 3a). The total sedimentary cover reaches a maximum thickness of 3.5 km within the largest graben at the southern slope of the Chatham Rise (between 130 to 170 km profile distance). Within the syn-rift sedimentary layers sed2 and sed3, P-wave velocities mostly increase gradually up to 4.9 km/s. Distinct reflections ($P_{sed2}P$ phase, Figures 4a and S1), however, indicate a stepwise increase of P-wave velocities between layers sed1 and sed2. Estimated uncertainties range between ±0.10 to ±0.20 km for sedimentary layer depths, and ±0.10 to ±0.20 km/s for the P-wave velocities within the layers (Table 1). Overall, the ray coverage is relatively low for the sedimentary layers (Figures 4a, 4b, and S1), but, as the MCS and wide-angle reflection/refraction data are in good agreement, we consider that the architecture of the sedimentary strata is well-resolved.

We divided the basement of the Chatham Rise and its southern slope into two upper crustal layers (Figure 3 and Table 1, layers uc1 and uc2). Both layers are well-resolved by P_{uc1} and P_{uc2} refraction phases (Figures 4b and 5). P-wave velocities indicate a minor change in the velocity gradient. Since the boundary between layer uc1 and uc2 is not reflective, it does not necessarily reflect a geological boundary. Layer uc1 is only present
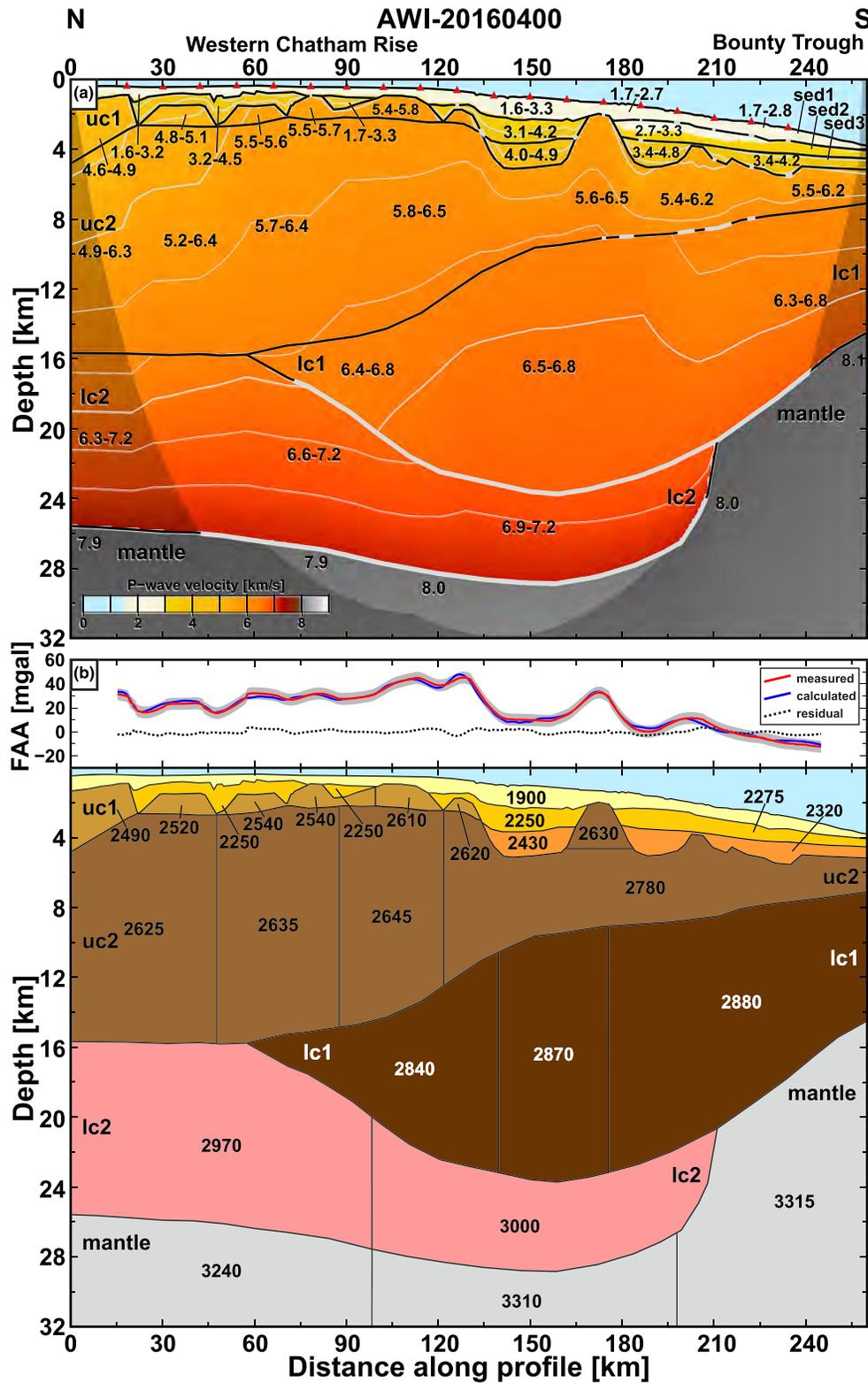
Figure 3. (a) P-wave velocity-depth model along profile AWI-20160400. The presented model is based on 20,530 picked arrivals. RMS travel time is 0.130 s with a corresponding χ^2 of 0.982. Detailed statistics on the P-wave velocity-depth model are shown in Tables S1 and S2. (b) Density-depth model from measured and modeled free-air gravity anomaly (FAA). Densities are given in kg/m^3.

Table 1
Layer Parameters and Corresponding Uncertainties Along AWI-20160400

Layer	Type	P-wave velocity range (km/s)	Velocity uncertainty (km/s)	Upper boundary uncertainty (km)	Densities/density range (kg/m^3)
Water layer					
0–260 km	Water	1.5	±0.01	0.00	1,020
Sediment 1 (sed1)					
0–170 km	Post-rift sed.	1.6–3.3	±0.10	±0.10	1,900
170–260 km	Post-rift sed.	1.7–2.8	±0.10	±0.10	1,900
Sediment 2 (sed2)					
0–170 km	Syn-rift sed.	3.1–4.2	±0.10	±0.10	2,250
170–260 km	Post- or syn-rift sed.	2.7–3.3	±0.15	±0.15	2,250–2,275
Sediment 3 (sed3)					
130–170 km	Syn-rift sed.	4.0–4.9	±0.20	±0.20	2,430
170–260 km	Syn-rift sed.	3.4–4.8	±0.20	±0.20	2,320
Upper crust 1 (uc1)					
0–135 km	Continental	4.6–5.8	±0.10	±0.10 to ±0.20	2,490–2,620
Upper crust 2 (uc2)					
0–120 km	Continental	4.9–6.5	±0.15	±0.15	2,625–2,645
120–260 km	Continental	5.4–6.5	±0.2	±0.20	2,780
Lower crust 1 (lc1)					
55–260 km	Continental	6.3–6.8	±0.20	±0.30	2,840–2,885[a]
Lower crust 2 (lc2)					
0–100 km	Oceanic plateau	6.3–7.2	±0.25	±0.30	2,970
100–215 km	Oceanic crust	6.9–7.2	±0.25	±0.40	3,000
Mantle					
0–100 km	Mantle	7.9–8.0	±0.30	±0.40	3,240
100–260 km	Mantle	8.0–8.1	±0.30	±0.40	3,310–3,315

Note. P-wave velocity and upper boundary uncertainties refer to relative uncertainties estimated from perturbation of the individual layers. P-wave velocities vary within one respective layer due to different geological settings and burial depths.
[a]Density is 2,650 kg/m^3 at the basement high between 165–180 km along profile.

along the crest of the Chatham Rise, where the total thickness of the upper crustal layers is up to 14.5 ± 0.2 km, between 0 and 135 km along profile (Figure 3). The thickness of layer uc2 continuously decreases across the Chatham Rise slope, reaching 2 ± 0.1 km at the border of the Bounty Trough. The absence of any reflection at the base of layer uc1 indicates that the P-wave velocities gradually increase from layer uc1 to uc2. Moreover, across the Chatham Rise, we find P-wave velocities and densities within these two upper crustal layers gradually increase from north to south toward the large graben at 135 km along profile (Figure 3).

We divided the lower crust of the Chatham Rise into two layers (Figure 3 and Table 1, layers lc1 and lc2) based on several reflection observed in the deep crust (Figure 5). Layer lc1 is present between ~60 and 260 km along profile (Figure 3a). Observed reflections ($P_{lc1}P$) indicate an abrupt increase of P-wave velocities along the upper boundary of layer lc1 (separating it from uc2) between 160 and 220 km along profile. Layer lc1 reaches its maximum thickness (~14 km) between 150 and 180 km along profile. In this area, we modeled the highest P-wave velocities (6.5–6.8 ± 0.2 km/s) that were moderately resolved by the P_{lc1} refraction phase (Figures 4b and 5). Layer lc1 thins significantly between 190 and 260 km along profile, reaching less than 8 ± 0.3 km by the southern slope of Chatham Rise (Figure 2a). While the P-wave velocities within layer lc1 decrease slightly toward the southern termination of the profile (6.3–6.8 km/s), gravity modeling suggests a gentle southward increase of densities in layer lc1 similar to the southward-increasing densities in the overlying layers uc1 and uc2 (Figure 2b). We find that the ranges of P-wave velocities and densities in layer lc1 are the same as those observed in the lower crust of the Chatham Rise along the seismic refraction profiles east of the Chatham Islands (AWI-20160100 and AWI-20160200; Riefstahl et al., 2020). The base of layer lc1 is defined by continuous high-amplitude reflections ($P_{lc2}P$; Figures 4 and 5) between 70 and 240 km along profile.

Later arrivals of another high-amplitude reflection (P_mP) and mantle refraction phase (P_n) imply another crustal layer lc2 below layer lc1 (Figure 2 and Table 1). Sparse refractions from layer lc2 recorded at one station suggest P-wave velocities higher than 6.3 ± 0.25 and 6.6 ± 0.25 km/s (Figure 2a). We estimated the
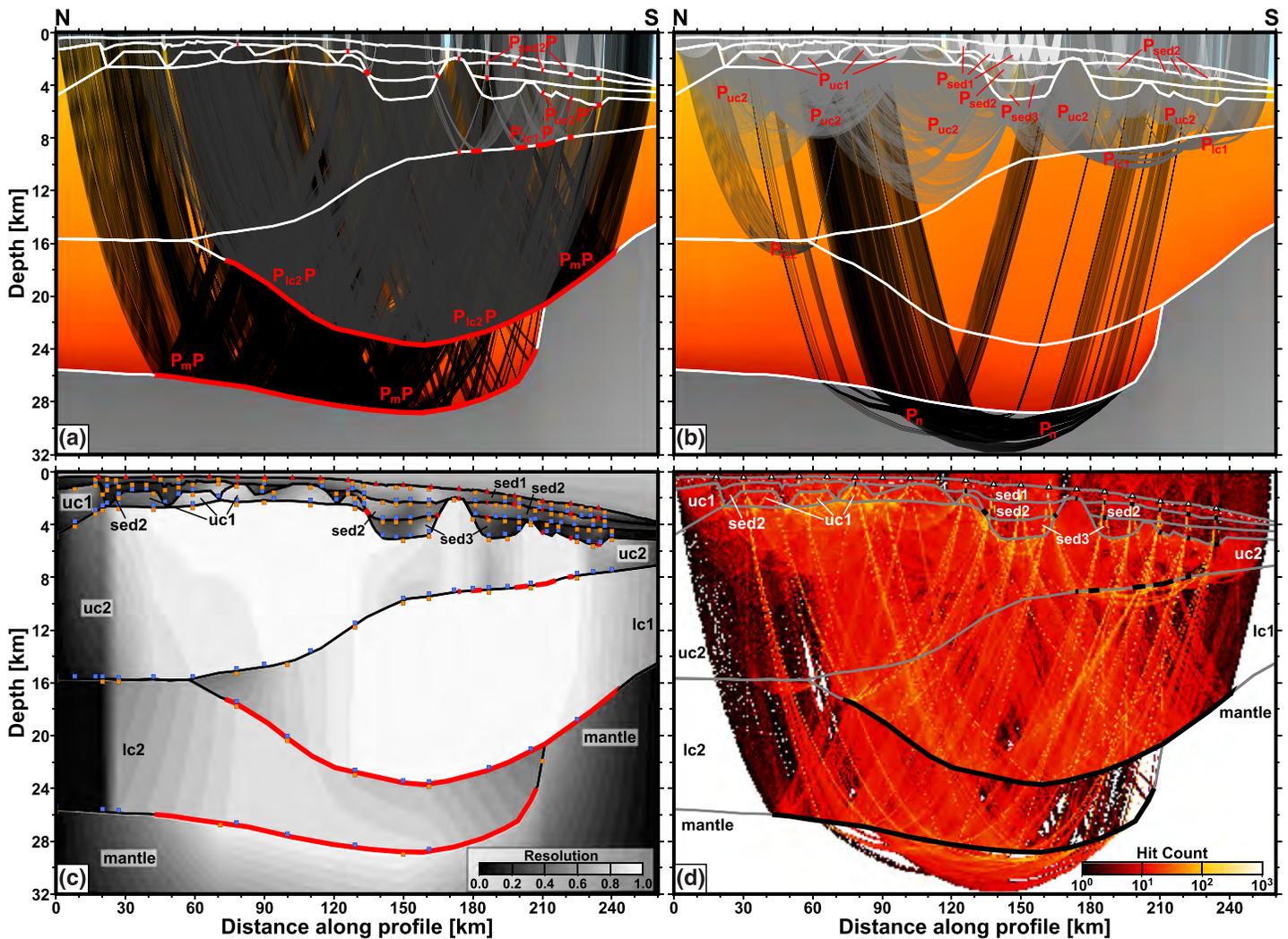
Figure 4. (a) Reflected ray phases, (b) refracted ray phases, (c) ray resolution (orange boxes = upper velocity nodes, blue boxes = lower velocity nodes), and (d) hit count along seismic refraction profile AWI-20160400. Red layer boundaries in (a) and (c) and black boundaries in (d) are reflective. Ray group coverage plots are illustrated in Figure S1.

P-wave velocities at the base of layer lc2 to be up to 7.2 ± 0.25 km/s using normal move-outs of the P_mP reflection phase. P-wave velocities higher than 7.0 km/s are in good agreement with densities of ~3,000 kg/m^3 as estimated from the gravity model (Figure 2b). The thickness of layer lc2 (~10 km) is approximately constant between 0 and 60 km along profile. Moreover, we find that the layer lc2 thins to less than 6 km thickness between 60 and 120 km along profile before disappearing ~210 km along profile, features which are well-resolved by continuously recorded $P_{lc2}P$ and P_mP phases (Figures 4b and 5).

We observe several P_n mantle refractions below the Chatham Rise and underthrusted Phoenix Plate (Figure 4b) and note a slight increase in their velocity from 7.9 km/s in the north to 8.1 km/s at the southern slope (Figure 2a).

5. Discussion

5.1. Structure of the Ancient Chatham Rise Accretionary Wedge

The half-graben and graben structures, which are obvious along the profile (Figures 2 and 3), correspond to regional free-air gravity anomalies along the Chatham Rise, which are mostly E-W oriented (Davy, 2014) parallel to the northern margin of the Chatham Rise and the Bounty Trough. These half-grabens are probably associated with thrust faults in the Chatham Rise accretionary wedge that may have been reactivated as
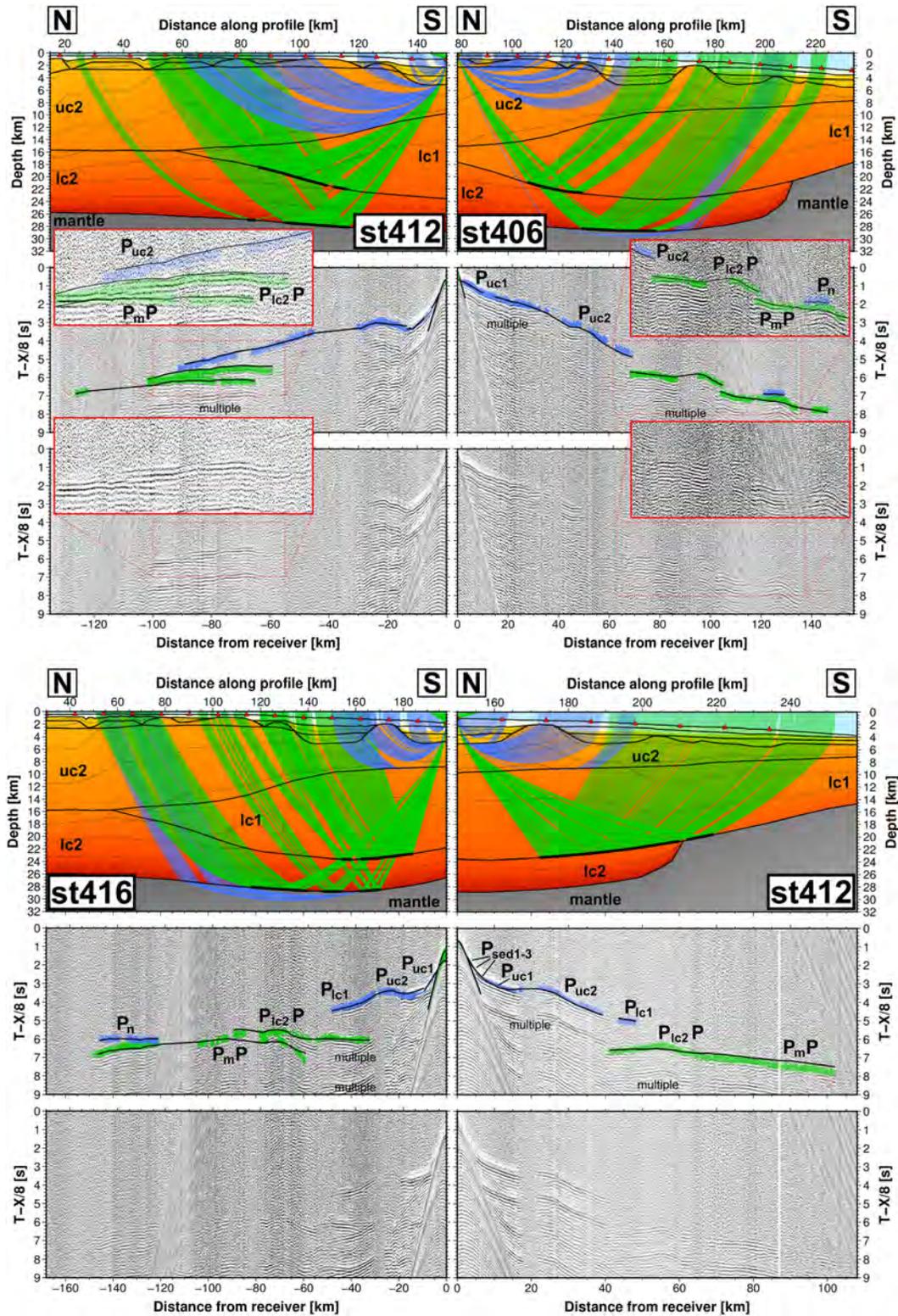
Figure 5. Ray tracing examples and OBS/OBH record for several stations demonstrating the presence of deep-crustal reflections along profile AWI-20160400. Thick black layer boundaries in the P-wave velocity models indicate reflection observed at the shown station. Blue rays indicate refracted wave phases, and green rays indicate reflected wave phases. Black lines in the seismograms are the modeled arrival times for all ray groups; vertical blue and green and green lines indicate the assigned uncertainty for each pick based on the signal-to-noise ratio.

normal faults after the onset of Zealandia rifting at around 105 Ma (Riefstahl et al., 2020; Tulloch et al., 2019). The larger graben and half-graben structures to the south are more likely related to rifting and progressive deepening of the Bounty Trough (Riefstahl et al., 2020). The oldest sediments within these graben structures may have an age of up to 100 Ma, similar to those from the Chatham Islands (Campbell et al., 1993).

We observed a north to south lateral gradient of P-wave velocities and densities in the upper crustal layers along our profile AWI-20160400 (Figure 3). A similar gradient has also been recognized along two wide-angle reflection/refraction profiles further east of the Chatham Islands (Riefstahl et al., 2020). We suggest that these N-S lateral P-wave velocity and density gradients are a result of regional metamorphism that affected the forearc of the Mesozoic arc, that is, the Chatham Rise area. Such regional metamorphism would be consistent with geological observations from the Chatham Islands (Mortimer, van den Bogaard, et al., 2019). Accordingly, rock assemblages consistent with the modeled P-wave velocities and densities range from sub- or lower greenschist facies (i.e., meta-graywackes to schists) in the north, to upper greenschist facies (mainly schist) in the southern part of profile AWI-20160400 (Figure 6a).

Furthermore, we observe model layer lc1 up to 14 km thick at 150–180 km along profile and thins out in southward toward the Bounty Trough, where it is less than 8 km thickness (Figure 3a). A lower crustal thickness of up to 14 km and P-wave velocities of 6.3–6.8 km/s are largely similar to the lower crust further east of the Chatham Islands (Riefstahl et al., 2020). Accordingly, we interpret layer lc1 as lower continental crust of the ancient Chatham accretionary wedge, which most likely consists of amphibolite facies gneiss with southward-increasing metamorphic grade (Figure 6a). This is also consistent with the southward-increasing metamorphic gradient of the overlying schists observed on the Chatham Islands (Mortimer, van den Bogaard, et al., 2019).

5.2. Southern Extent and Thickness of the Hikurangi Plateau

The lower crustal layer lc2, which is 10 km thick between 0 and 60 km along profile (Figure 3a), thins to 6 km thickness by ~100 km along profile. Gravity modeling suggests higher densities of 2,970 kg/m^3 (Figure 3b). Close to our profile, the top of the Hikurangi Plateau has been observed along the MCS reflection profile HKDC-1 at 6–7 s two-way traveltime (Davy et al., 2008). In contrast, we found no evidence for any reflections separating layers lc2 and uc1 between 0 and 60 km along our profile due to poor seismic penetration in that area. Assuming an average velocity of 5,500 km/s, we would expect the top of the Hikurangi Plateau observed along line HKDC-1 to be at a depth of 16.5–19.25 km. This is close to the modeled the top of our layer lc2 at 16 km depth. Further to the east, higher densities have been also observed along two profiles where the underthrusted Hikurangi Plateau is expected (Riefstahl et al., 2020). Accordingly, we interpret this part of layer lc2 between 0 and 100 km profile as the underthrusted Hikurangi Plateau beneath the Chatham Rise accretionary wedge.

We compare the results of our P-wave velocity-depth and gravity models with other observations of the extent of the Hikurangi Plateau and adjacent oceanic crust beneath the Chatham Rise and southern Zealandia region (Figure 6). The 10 km thickness of the Hikurangi Plateau underlying the Chatham Rise implied by our P-wave velocity-depth model along profile AWI-20160400 is in very good agreement with thicknesses between 10 and 12 km derived from (i) gravity models along HKDC-1 line (Figure 7; Davy et al., 2008); (ii) the AWI-20160100 seismic refraction profile east of the Chatham Islands (Figure 6c; Riefstahl et al., 2020); and (iii) seismic refraction profiles from the northern Hikurangi margin east of the North Island (Figure 7; Henrys et al., 2013; Herath et al., 2020; Mochizuki et al., 2019, Scherwath et al., 2010; Tozer et al., 2017). The available data from the Hikurangi Plateau do not suggest large variations in thickness along the Chatham Rise between 175°E to 176°W. In contrast, further to the east, at the eastern margin of the Plateau, seismic reflection data and gravity models crossing the WWR (Figure 7; Barrett et al., 2018), as well as seismic refraction profile AWI-20160200 at the southward extension of the WWR on the Chatham Rise (Figure 6b; Riefstahl et al., 2020), indicate that the Hikurangi Plateau thickens to 12–16 km. This thickening of the Hikurangi Plateau along its eastern margin is likely due to either complex dextral strike-slip movements along the WWR, where compressional and extensional features are in close proximity to each other (Barrett et al., 2018); massive volcanic activity during stretching and rifting from the conjugate Manihiki Plateau (Hochmuth et al., 2015); or reflect natural variations in the crustal thickness of oceanic plateaux (e.g., Hochmuth et al., 2019).
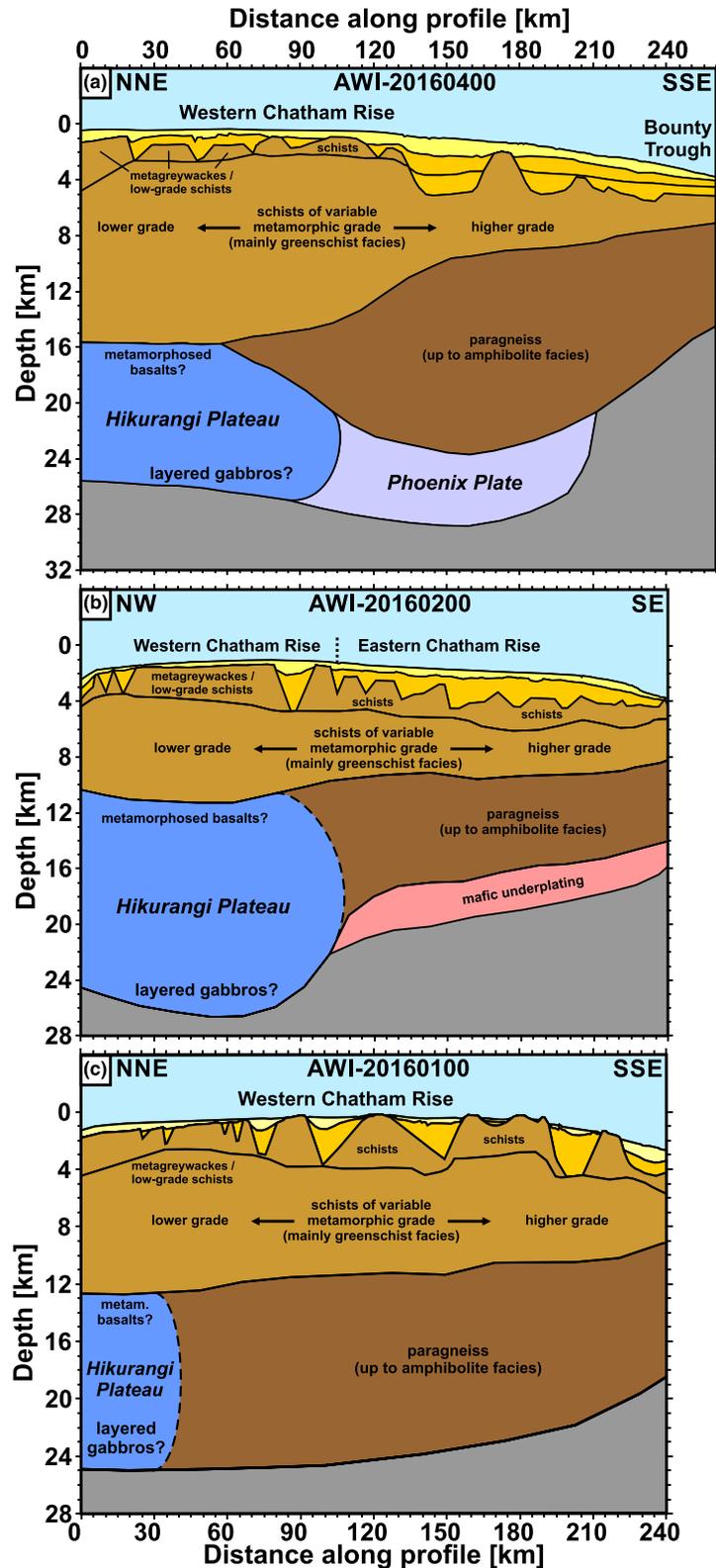
Figure 6. Geological interpretation along seismic refraction profile (a) AWI-20160400 as well as the northern parts of profiles (b) AWI-20160200 (Riefstahl et al., 2020) and (c) AWI-20160100 (Riefstahl et al., 2020) indicating the extent of the underthrusted Hikurangi Plateau beneath the western Chatham Rise. The locations of the presented profiles are shown in Figure 7.
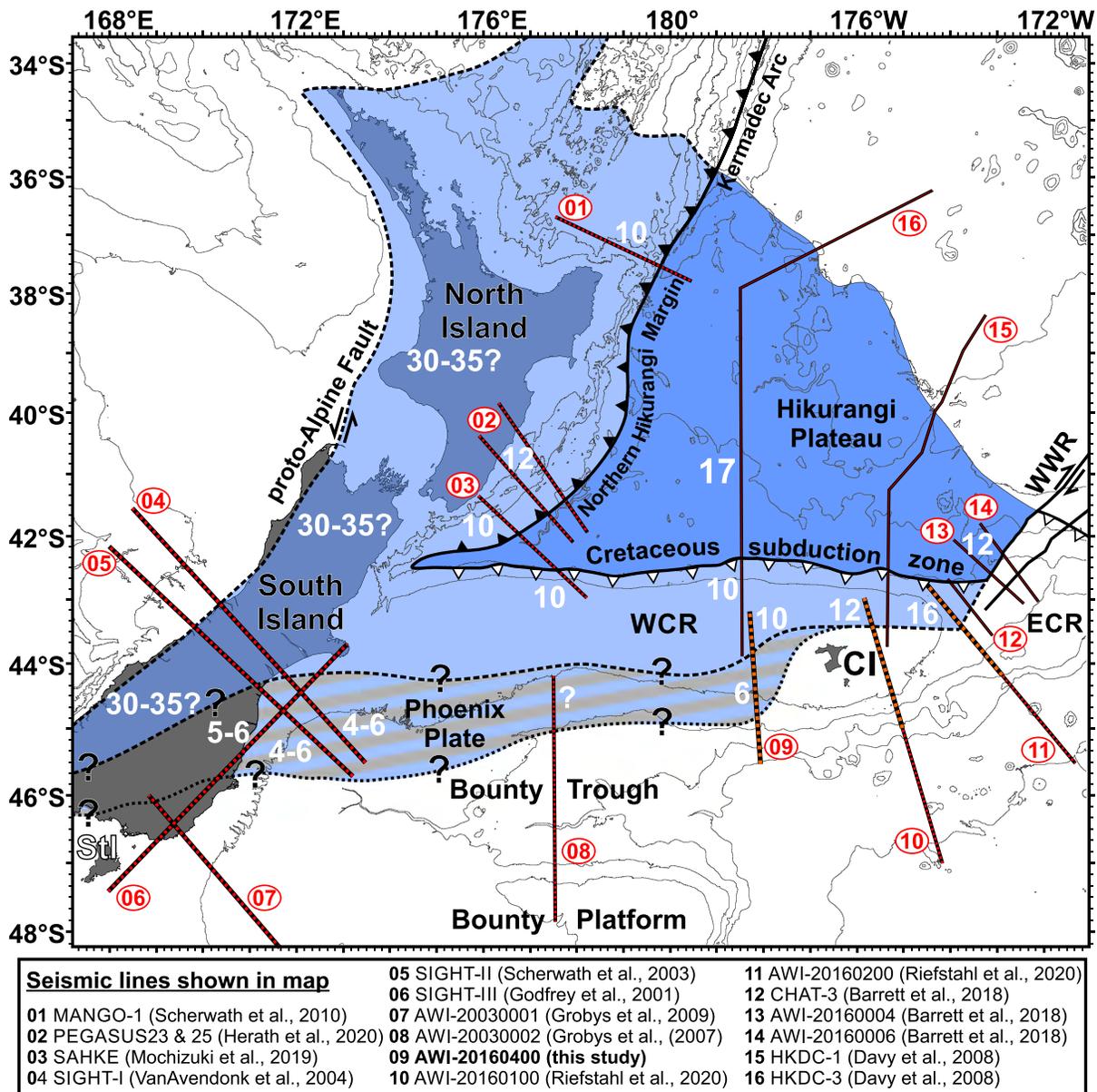
Figure 7. Map showing the extent of the Hikurangi Plateau (transparent blue) and subducted Phoenix Plate oceanic crust (transparent hatched grayish-blue) with estimated thicknesses (in km) beneath Zealandia. High thickness estimates of 30–35 km for the Hikurangi Plateau are from seismological V_p and V_p/V_s models of Reyners et al. (2011) and Reyners et al. (2017). Thicker and orange colored profiles (09-11) are shown in Figure 6. The mid-Cretaceous STEP faults, which became active in response to subduction jamming are represented by the dextral West Wishbone Ridge (WWR) and the sinistral proto-Alpine Fault. CI = Chatham Islands, ECR = eastern Chatham Rise, StI = Steward Island, WCR = Western Chatham Rise.

The extent of the subducted Hikurangi Plateau beneath the North Island and South Island was previously illustrated using seismological V_p and V_p/V_s models (Reyners et al., 2011, 2017). Beneath the eastern South Island, the Hikurangi Plateau has been inferred to dip steeply westward to a depth of 65–100 km, where it eventually collides with the eastward down-dipping slab of the Australian Plate along the southwest side of the South Island (Reyners et al., 2017). Here, the Hikurangi Plateau is interpreted to be 30–35 km thick (Figures 6a–6c; Reyners, 2013; Reyners et al., 2017). However, how the base of the Hikurangi Plateau is defined is important. Reyners et al. (2017) considered P-wave velocities around 8.5 km/s or higher (=eclogitization?) observed from a seismological network as a proxy for the subducted Hikurangi Plateau. This approach is based on observation from seismic refraction studies, which noted similar high or even

higher P-wave velocities observed below the 40 km thick Ontong Java Plateau (Furumoto et al., 1976). On the basis of a seismic refraction experiment crossing the northern Hikurangi margin (seismic profiles PEGASUS23 & 25, Figure 7), Herath et al. (2020) argued this high thickness of the Hikurangi Plateau beneath both the North and South Islands. In their study, they identified a double seismic zone in the mantle beneath the Hikurangi Plateau, with an increase of P-wave velocities in the mantle from normal mantle velocities of 8.0–8.3 km/s to ~8.7 km/s in 50–60 km depth—around 25 km below the Hikurangi Plateau of 10–12 km thickness. This high P-wave velocity may be related to aggregates of olivine related to the plume below the Ontong Java Nui super-plateau (Stern et al., 2020). However, Herath et al. (2020) suggested that Reyners (2013) and Reyners et al. (2017) had included the mantle with normal mantle velocities of 8.0–8.3 km/s above this high-velocity zone in their crustal thickness estimates of the Hikurangi Plateau.

In this study, we define P-wave velocities higher than 7.9–8.0 km/s as the mantle, which is clearly separated from the Hikurangi Plateau and Chatham Rise crust by a distinct P_mP (Moho) reflection. This is similar to the eastern and thinner Chatham Rise (Figure 6), where only the Phoenix Plate, and not Hikurangi Plateau, was not subducted (Barrett et al., 2018; Riefstahl et al., 2020). We do not rule out that the Hikurangi Plateau may be thicker below the North and South Islands than beneath the Chatham Rise, as the western part of the Hikurangi Plateau was closer to the Ontong Java Nui eruption center (Hochmuth et al., 2015). The Ontong Java Plateau constitutes the Earth's thickest known oceanic plateau crust (Furumoto et al., 1976). In contrast, the Manihiki Plateau at a greater distance from the Ontong Java Nui eruption center is not thicker than 20 km (Hochmuth et al., 2019). Moreover, large parts of the western Manihiki Plateau are between 9 and 17 thick (Hochmuth et al., 2019), which correlates with the thickness of the Hikurangi Plateau beneath the Chatham Rise (this study; Mochizuki et al., 2019; Riefstahl et al., 2020). Accordingly, we consider our modeled thickness of 10 km for the Hikurangi Plateau below the Chatham Rise as very meaningful.

5.3. Extent and Age of the Phoenix Plate

Based on the observed deep-crustal reflection (Figure 5), our P-wave velocity-depth model suggests that layer lc2 thins between 60 and 120 km along profile from 10 km to only ~6 km thickness. We interpret this as the transition from the Hikurangi Plateau to normal, ~6 km thick oceanic crust: the ancient Phoenix Plate (Figure 6a). An alternative explanation would be that the southern part of layer lc2 is part of the Hikurangi Plateau that was stretched prior to slab detachment. We suggest that this is unlikely as the thickness of layer lc2 is approximately constant (~6 km) between 120 and 180 km along profile. P-wave velocities and densities are also in the range of magmatic mafic underplating. Mafic underplating of much less thickness (only 2 km) has been interpreted further west along AWI-20160200 at the eastern Chatham Rise (Figure 6b; Riefstahl et al., 2020). The location crosses the central part of the Chatham Rise, and we would only expect magmatic underplating in areas where the crust is much thinner.

Based on seismological studies of the South Island, Reyners et al. (2011) suggested that the whole Chatham Rise is underlain by the Hikurangi Plateau. However, the results of modeling along our combined MCS, gravity, and wide-angle seismic reflection/refraction profile AWI-20160400 (Figures 2 and 3a)—together with interpreted MCS and wide-angle seismic reflection/refraction profiles east of the Chatham Islands (Riefstahl et al., 2020) (Figures 6b and 6c)—show that the underthrusted Hikurangi Plateau reaches only approximately half the full N-S lateral extent of the Chatham Rise. Moreover, we find evidence along AWI-20160400 that the oceanic crust of the leading Phoenix Plate is still attached to the Hikurangi Plateau beneath the central Chatham Rise (Figure 6a); this oceanic crust, however, is detached further east (Figures 6b and 6c; Riefstahl et al., 2020).

Seismological studies of the southeastern South Island highlight the presence of westward-dipping oceanic crust in the mantle (Reyners et al., 2017). We suggest that this oceanic crust beneath the South Island (Figure 7) is the continuation of the Phoenix Plate oceanic crust that we observe beneath the Chatham Rise (Figure 6a). Oceanic crust has also been identified beneath the highly extended continental crust underlying the Cretaceous sedimentary basins east of the South Island and west of our profile AWI-20160400 (Figure 7; SIGHT-I/II/III; Godfrey et al., 2001; Scherwath et al., 2003; Van Avendonk et al., 2004) but also potentially below the continental crust of the South Island (Smith et al., 1995). Godfrey et al. (2001) suggested that this is the crust on which the forearc terranes accumulated. In contrast, we suggest that this oceanic crust is part of the Phoenix Plate, which we interpret from our profile.

East of these basins, gravity anomalies within the inner Bounty Trough have been interpreted to reflect the southern extent of the Hikurangi Plateau and/or oceanic crust (Davy, 2014). Our model derived from the combined refraction seismic and gravity data along profile AWI-20160400 does not directly indicate the presence of oceanic crust in the inner Bounty Trough. Between our profile and the inner Bounty Trough, neither subducted oceanic crust nor remnants of Hikurangi Plateau have been recognized below the 21-km-thick Chatham Rise by the only seismic refraction line crossing the Bounty Trough (Figure 7; Grobys et al., 2007). However, the northern termination of seismic line AWI-20030002 has very limited ray coverage at the southern Chatham Rise margin (Grobys et al., 2007). Accordingly, the presence of oceanic crust at the northern limit of the Bounty Trough west of our profile AWI-20160400 cannot be ruled out. If oceanic crust is present in that area, it implies that a piece of the ancient Phoenix Plate extending ~1,200 km from east to west is still attached to the southern edge of the Hikurangi Plateau (Figure 7).

Determining the southward extent of the Phoenix Plate beneath southern Zealandia is challenging. V_p and V_p/V_s models of the South Island indicate that eclogitized oceanic crust is present until or even below the Median Batholith (Reyners et al., 2017)—the ancient volcanic arc of the former East Gondwana subduction zone that is located beneath the southernmost South Island and Stewart Island (Figure 7). However, interpretations of the seismic refraction line SIGHT-III that runs east of and parallel to the South Island (Godfrey et al., 2001) suggest that "old" oceanic crust is limited to the area north of the Median Batholith. This provides a possible southern limit to the extent of the Phoenix Plate oceanic crust in the vicinity of the South Island and explains why oceanic crust has not been observed along the seismic refraction line AWI-20030001, located southeast of the South Island (Figure 7; Grobys et al., 2009). As the widely rifted continental Bounty Trough is apparently not underlain by oceanic crust (Grobys et al., 2007), we suggest that the southern limit of the Phoenix Plate corresponds with the southern margin of the Chatham Rise, as inferred by Davy (2014) from variations in gravity gradient fabrics in the inner Bounty Trough. With this constraint, we find that the N-S extent of the Phoenix Plate attached to the Hikurangi Plateau varies between 100 and 200 km but probably does not exceed more than 200 km south of the underthrusted Hikurangi Plateau.

Because most of its oceanic crust was subsequently subducted during the mid-Cretaceous, the age and much of the spreading history of the Phoenix Plate are unknown (Seton et al., 2012). It is thought that the Ontong Java Plateau, northwest of the Hikurangi Plateau, was emplaced on or beside oceanic crust that formed between M29 (~156 Ma) and M0 (~120 Ma) along the Pacific-Phoenix spreading ridge (e.g., Hochmuth et al., 2015; Seton et al., 2012). Accordingly, the piece of subducted Phoenix Plate that we have identified below the Chatham Rise is most likely older than the emplacement of Ontong Java Nui at 125–120 Ma (Hoernle et al., 2010; Taylor, 2006). Considering recent plate tectonic reconstructions and spreading anomalies (Hochmuth & Gohl, 2017; Hochmuth et al., 2015; Matthews et al., 2012; Seton et al., 2012), the piece of the Phoenix Plate south of the Hikurangi Plateau is likely not, or not much, older than the M29 spreading anomaly (~156 Ma).

5.4. Plateau Collision/Underthrusting, Slab Flattening, and Onset of Extension

In our conceptual model (Figure 8), we envisage the subducting oceanic Phoenix Plate as a shallow slab in the pre-collisional setting before 105 Ma. This is based on changing geochemical/isotopical compositions of subduction-related granitoids within the Median Batholith onshore South Island, which indicate shallow mantle wedge melting, and thermochronological data, which suggest a continent-ward migration of the arc after 125 Ma (Tulloch & Kimbrough, 2003). This may be related to younger oceanic slab entering the trench (van Hunen et al., 2002) and would be in agreement with a young age for the Phoenix Plate during the evolution of the OJP (Hochmuth et al., 2015) that was then subducted along the East Gondwana margin. Another explanation for shallow subduction after 125 Ma would be that seafloor spreading between Manihiki and Hikurangi Plateau was very fast (~190 mm/year, Zhang & Li, 2016). In modern subduction zones, the distance between arc and trench (width of the accretionary wedge and forearc area) is mainly within 100–300 km (Dickinson, 1973). Along the East Gondwana margin the arc-trench distance most likely exceeded the modern 300 km, which is consistent with geological observations from the South Island (e.g., Jacob et al., 2017).

A dramatic change of tectonic forces affected Zealandia during the mid-Cretaceous, with the previous compressional regime being replaced by widespread extension (Bradshaw, 1989; Laird & Bradshaw, 2004). The
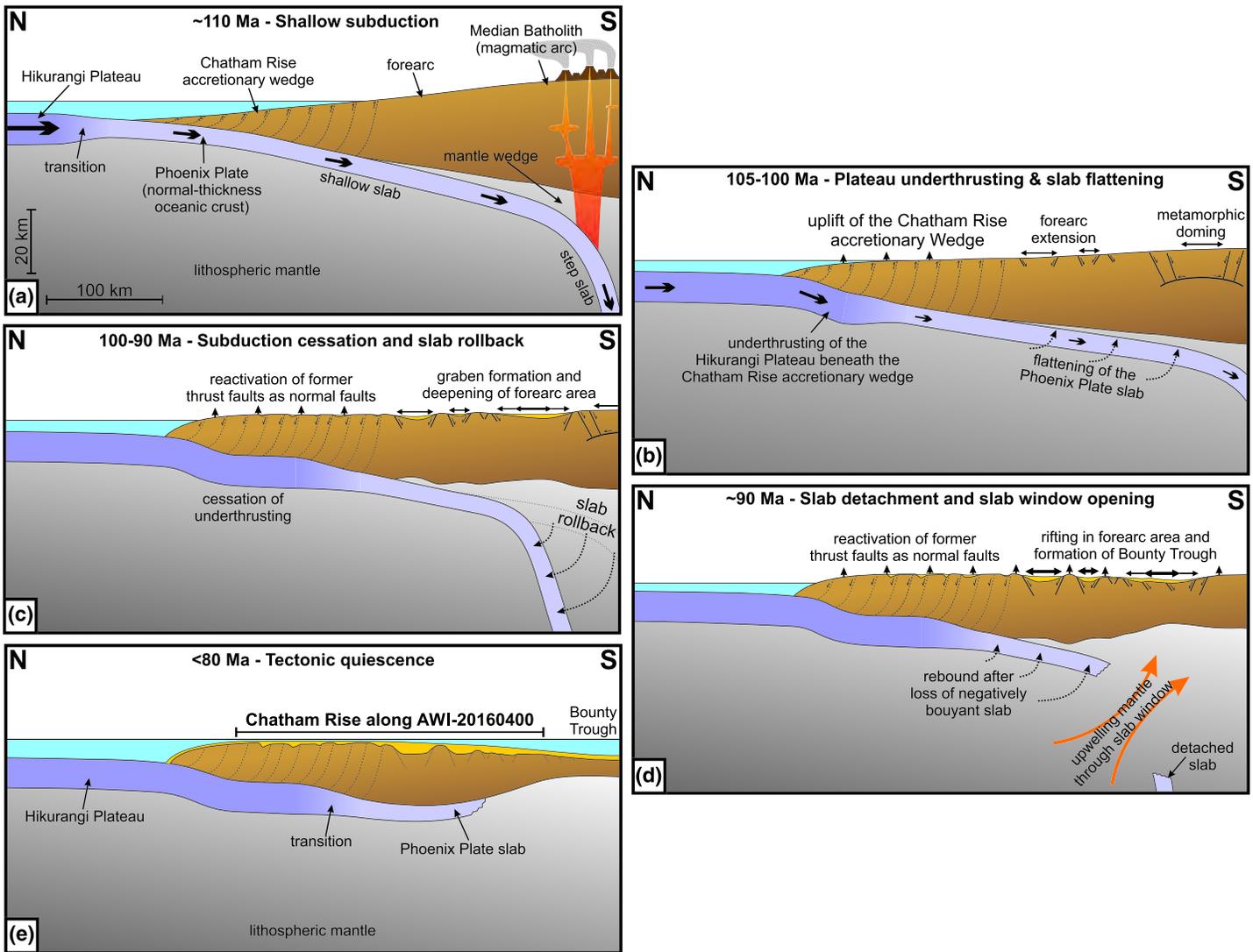
Figure 8. Conceptual model of the Hikurangi Plateau underthrusting and subsequent slab processes along the Chatham Rise between the initial Hikurangi Plateau collision and subduction at ~110 Ma and the final separation of southern Zealandia and West Antarctica at ~80 Ma. See text for further explanations.

end of long-lived subduction along the East Gondwana margin was initiated when the Hikurangi Plateau entered the subduction zone between 110 and 100 Ma (Davy, 2014; Davy et al., 2008). Our conceptual model is consistent with earlier tectonic models inferring that the Hikurangi Plateau started to collide and subduct from the NNW beneath the South Island and western Chatham Rise at 110 Ma and beneath the eastern Chatham Rise at 105–100 Ma (Figure 8b; Davy, 2014; Reyners et al., 2017).

The part of the Hikurangi Plateau that first entered the trench was most likely the part that is now located in the mantle beneath the southernmost South Island (Reyners et al., 2017). In contrast with normal oceanic crust, over-thickened volcanic oceanic plateaux like the Hikurangi Plateau have insufficient negative buoyancy to be subducted without consequences for margin deformation and convergence rate (Cloos, 1993; Espurt et al., 2008; van Hunen et al., 2002). An oceanic plateau of even 12 km thick remains positively buoyant until an age of around 80 Myr, and thicker plateaux are positively buoyant for even longer (van Hunen et al., 2002). In response to the onset of subduction of the thicker part of the Hikurangi Plateau in the area of the South Island at 110 Ma, the convergence rate in this region slowed down. Further east, beneath the Chatham Rise, subduction of the oceanic Phoenix Plate continued at least until 105 Ma, and the convergence rate in this region was, therefore, higher. This asymmetry likely led to the proposed clockwise rotation of the

East Gondwana margin in the Chatham Rise region (Davy, 2014; Reyners et al., 2017). In response, the direction of seafloor spreading north of the Hikurangi Plateau rotated from NNW-SSE to approximately N-S (Davy, 2014; Davy et al., 2008; Downey et al., 2007). Initial subduction of the eastern, thinner (~10-km thick) part of the Hikurangi Plateau led to progressive southward uplift of the accretionary wedge, that is, the northern Chatham Rise margin (Figure 8b). We speculate that the positive buoyancy of the thicker Hikurangi Plateau, which subducted far more southward below the South Island, may have initiated further flattening of the attached Phoenix Plate slab to the east after the onset of subduction and underthrusting of the Hikurangi Plateau. Both the slab flattening and decreasing convergence velocity may explain the abrupt cessation of arc construction processes, and the onset of metamorphic doming and extensional collapse between 108 and 106 Ma (Figure 8b; Schwartz et al., 2016). Crustal extension in the forearc area of the East Gondwana margin—the "Zealandia Rift Phase"—then began after ca. 105 Ma, as evidenced by the evolution of mid-Cretaceous graben-controlled rift basins around New Zealand (Strogen et al., 2017). On the Chatham Islands, low-temperature thermochronological data indicate rapid cooling from at least 108 ± 11 Ma (four ZHe ages) to 80 ± 14 Ma (only one AFT age) (Mortimer et al., 2016). This illustrates that several kilometers of rock denudation—leading to exhumation of schists on the Chatham Islands—was most likely already ongoing or initiated after the Hikurangi Plateau subduction. Flattening of the Phoenix Plate slab (Figure 8b) may have led to uplift in the accretionary wedge and forearc area (Espurt et al., 2008), that is, the Chatham Rise. We speculate that the slab flattening was triggered by the progressing subduction of the Hikurangi Plateau in the area of the South Island since 110 Ma. This may have also initiated extension in the forearc area. A second factor, which eventually produced extension along the Chatham Rise, may be the counter-clockwise rotation of the East Gondwana margin (Davy, 2014; Reyners et al., 2017). Additionally, transfer of dextral motions along the WWR and divergence of these dextral motions through smaller fault system may have also played a role in facilitating extension along the eastern part of the Chatham Rise (Barrett et al., 2018; Davy, 2014).

5.5. Development of STEP Faults and Slab Rollback

Subduction presumably continued both east and west of the Hikurangi Plateau (Mortimer et al., 2019), leading to the development of Subduction-Transform Edge Propagator (STEP) faults (Govers & Wortel, 2005). The last remnants of oceanic crust west of the Hikurangi Plateau were completely subducted at the Australian-Pacific plate boundary in the Eocene (Reyners, 2013). However, the presence of alkaline intra-plate magmatism in Marlborough and Westland onshore of the South Island shortly after 100 Ma implies that a slab window or tear opened along the sinistral STEP fault at the western edge of the Hikurangi Plateau (Hoernle et al., 2020; van der Meer et al., 2016, 2017). Since this STEP is close to the present-day Alpine fault, we also refer it as proto-Alpine Fault (Figure 7) according to van der Meer et al. (2016). East of the Hikurangi Plateau, subduction continued and was compensated by another STEP fault that has remained as the prominent dextral WWR (Figures 1a and 7; Barrett et al., 2018; Davy, 2014; Davy et al., 2008; Riefstahl et al., 2020), which is inferred to have first become active after 105 Ma (Barrett et al., 2018). Along the northeastern Chatham Rise margin east of the WWR, oceanic crust of the Phoenix Plate continued to subduct until at least 100 Ma (Riefstahl et al., 2020). We suggest that the slab of the Phoenix Plate south of the Hikurangi Plateau became decoupled from the Phoenix Plate slabs to the east and to the west after both STEP faults became active. Although subduction slowed and finally ceased due to blockage by the buoyant Hikurangi Plateau, eclogitization and associated densification of the steeper, arc-ward Phoenix Plate slab are likely to have continued (Duesterhoeft et al., 2014; Huangfu et al., 2016; Li et al., 2013). The additional negative buoyancy of progressive eclogitization will have continued to pull down the Phoenix Plate slab and led to slab rollback along the Hikurangi Plateau segment of the Phoenix Plate. This would have triggered further rifting and focused extension, which is expressed by graben formation and successive deepening of the forearc in the area that later formed the Bounty Trough (Figure 8c). Moreover, this enabled the lower lithosphere to heat up to granulite facies conditions, as evidenced by granulite xenoliths with peak metamorphic ages of 91.7 ± 2.0 Ma that were collected in Otago in the South Island (Jacob et al., 2017). We suggest that a ca. 97 Ma A-type granite from the Chatham Rise (Mortimer et al., 2006) is also related to this event. Synchronously with the cessation of subduction at the Chatham Rise, seafloor spreading north of the Hikurangi Plateau either ceased (Davy, 2014), or continued at a slower rate until 79 Ma (Mortimer, Campbell, & Moerhuis, 2019).

5.6. Slab Detachment and Focus of Rifting in the Bounty Trough

Seismic studies of northern and southern Zealandia's basement indicate multi-directional normal faulting (NE-SW, E-W, NW-SW), which was active between at least 105 to 85 Ma (Barrier et al., 2020). In southern Zealandia, the major direction of extension likely rotated by ~60° from NE-SW (orthogonal to the then-active East Gondwana margin; Davy, 2014) to NW-SE (approximately orthogonal to the Pacific-Antarctic ridge active after ~85 Ma) at around 90 Ma as indicated (Tulloch et al., 2019). This is consistent with the timing of onset of rifting in the Bounty Trough (Figure 8) inferred by most plate tectonic reconstructions (Eagles et al., 2004; Larter et al., 2002; Wobbe et al., 2012). This second stage of the "Zealandia Rift Phase" resulted in the formation of oceanic crust between the eastern Chatham Rise and eastern Marie Byrd Land of West Antarctica (Eagles et al., 2004; Larter et al., 2002; Riefstahl et al., 2020; Wobbe et al., 2012). We suggest that the observed change in the direction of extension may have been triggered by detachment of large proportions of the subducted Phoenix Plate slab at ~90 Ma, approximately 15–20 Myr after the initial collision and onset of underthrusting of the Hikurangi Plateau beneath the Chatham Rise. This probably initiated the final stage of the development of Bounty Trough. The delay time between the initial collision and subsequent slab detachment depends mostly on the strength of the previously subducted oceanic plate. 3-D numerical models indicate that typical delay times range from more than 20 Myr for old and strong slabs, to 10 Myr for very young and weak slabs (van Hunen & Allen, 2011). Correspondingly, slab detachment 15–20 Myr after the collision of the Hikurangi Plateau with the Chatham Rise is not unreasonable.

Numerical models suggest that significant asymmetry in a collisional setting leads to slab detachment that preferentially begins near one edge of the slab (van Hunen & Allen, 2011). We suggest that slab tearing beneath the Chatham Rise began at the southwestern leading edge of the Hikurangi Plateau close to the already evolved western STEP fault, which is linked to alkaline intraplate magmatism that affected parts of the northern and western South Island shortly after 100 Ma (Figure 8; Hoernle et al., 2020). Here, the transition between the thicker, more buoyant crust of the Hikurangi Plateau and the thinner oceanic crust of the Phoenix Plate would mechanically favor slab necking and detachment (Baumann et al., 2010). Low convergence rates after the Hikurangi Plateau collision would have led to a shallower depth (%3C100 km) for the slab detachment (Huangfu et al., 2016). The slab tear presumably migrated eastward into the interior of the Phoenix Plate where we infer the Phoenix Plate segment to be present on profile AWI-20160400 (Figure 6a).

As for the delay time between collision and slab detachment, propagation of slab tears also depends on the strength and age of the oceanic crust (van Hunen & Allen, 2011). Assuming that this part of the Phoenix Plate was already ~60 Myr old, the tear propagation speed would be ~300 km/Myr (van Hunen & Allen, 2011). This implies that the Phoenix Plate slab south of the Hikurangi Plateau was fully detached within 5 Myr of the onset of slab tearing. The loss of the deeper, steeply dipping, and presumably largely eclogitized slab of the Phoenix Plate—and the corresponding loss of negative buoyancy—would have caused the shallower Phoenix Plate slab and the buoyant Hikurangi Plateau crust to rebound (Duretz et al., 2011; Edwards et al., 2015; Gerya et al., 2004) and "underplate" the thin Chatham Rise continental accretionary wedge and forearc crust (Figure 8d). Moreover, the loss of a large segment of the oceanic Phoenix Plate by slab detachment, together with rebound of the remaining slab, will have triggered a regional dynamic topographic response along the East Gondwana margin (Duretz et al., 2011; Wortel & Spakman, 2000). A slab detachment can also cause crustal extension as proposed for the India-Eurasia collision (Magni et al., 2017). The margin uplifted and extension focused in the forearc area, which most likely intensified rifting and led to the formation of the Bounty Trough by ca. 80 Ma, when westward-propagating seafloor spreading finally separated southern Zealandia from West Antarctica (Figure 8d; Riefstahl et al., 2020).

Slab tearing created a pathway for mantle upwelling, which affected the evolving southern Zealandia rifted margin around 85 Ma (Hoernle et al., 2020; Riefstahl et al., 2020; Tulloch et al., 2019). Alkaline magmatism occurred on the Chatham Islands between 86 and 79 Ma (Panter et al., 2006) and at several seamounts further to the south and west of the Chatham Islands (Hoernle et al., 2020; Homrighausen et al., 2018; Mortimer, Campbell, & Moerhuis, 2019). Isotopic constraints of this intraplate volcanic event indicate a common HIMU end-member across multiple volcanic provinces in southern Zealandia (Hoernle et al., 2020) and suggest that the same deep-mantle source was involved in the evolution of the alkaline volcanic provinces located on the South Islands Marlborough (98–69 Ma; McCoy-West et al., 2010; Mortimer,

Campbell, & Moerhuis, 2019; van der Meer et al., 2016, 2017) and seamounts on the Hikurangi Plateau (99–86 Ma; Hoernle et al., 2010). If the mantle was already upwelling beneath the Hikurangi Plateau and the Phoenix Plate at or before 100 Ma, this could have also contributed to shallow subduction and flattening of the Phoenix Plate slab before 100 Ma (Figure 8b). This may be comparable with the central Andes, where a plume is suggested to have resulted in shallow and flat subduction (Gianni et al., 2017). A low-velocity zone in the mantle has also been identified in the Peruvian Andes below its prominent flat slab segment (Bishop et al., 2017). Although alkaline volcanism in southern Zealandia was apparently spatially limited and of low volume, magnetic anomalies in the region suggest that it affected larger areas (Tulloch et al., 2019).

5.7. Plate Tectonic Implications

A global-scale plate reorganization event, inferred to have occurred between 105 and 100 Ma, is thought to be the cause for fracture zone bendings and terminations preserved in all ocean basins, as well as the trigger for changes in the tectonic regimes like thrusting initiation, transpression and basin inversions (Matthews et al., 2012). Following Bradshaw (1989) and Luyendyk et al. (2001), Matthews et al. (2012) argued that the subduction of a spreading ridge along the East Gondwana margin initiated this event and the changing tectonic regime in the region of the Zealandia continent. Contrastingly, Davy (2014) and Reyners et al. (2017) proposed that the cessation of subduction along the East Gondwana margin in response to jamming by the Hikurangi Plateau initiated the plate reorganization and the transformation from subduction to extension. Recent research suggests that this mid-Cretaceous global plate reorganization event already commenced at ~111 Ma following to a slab detachment in the Mesotethys Ocean (Olierook et al., 2020).

Geodynamic modeling suggests that the slab width has significant first-order effects on plate kinematic processes (Schellart et al., 2007). Cessation of subduction in response to underthrusting of the Hikurangi Plateau would have split the ultra-wide subduction zone—which, at that time, extended across New Guinea, Australia, Zealandia, West Antarctica, and South America (e.g., Matthews et al., 2016)—into two narrower subduction zones east and west of the Hikurangi Plateau. We suggest that this fragmentation of the East Gondwana subduction zone and Phoenix Plate—the major consequence of the cessation of subduction of the Hikurangi Plateau—significantly contributed to and prolonged the ongoing global plate reorganization event between 105 and 100 Ma. Our study highlights that oceanic plateau subduction, underthrusting and subduction zone jamming can result in various local, regional, and global effects with significant consequences.

6. Conclusions

In this study, we present newly acquired seismic refraction/wide-angle reflection, MCS reflection, and potential field data along a profile across the submarine Chatham Rise, offshore New Zealand. Our P-wave velocity and gravity modeling reveal the crustal structure of the Chatham Rise west of the Chatham Islands. The models provide new insights into the former East Gondwana subduction zone, which was blocked by subduction and underthrusting of the Hikurangi Plateau in the mid-Cretaceous.

P-wave velocities for the continental part of the Chatham Rise accretionary wedge suggest a composition similar to that observed elsewhere on the Chatham Rise: mainly meta-graywackes, schist, and high-metamorphic equivalents. Our P-wave velocity and density models indicate that the southernmost extent of the underthrusted Hikurangi Plateau is less than 200 km from the northern border of the Chatham Rise. Moreover, a piece of the ancient Phoenix Plate is still attached south of the Hikurangi Plateau. Linking our observations with published geophysical data, we suggest that this piece of oceanic crust extends from east of the Chatham Islands to the South Island of New Zealand (up to 1,000 × 250 km).

On the basis of our observations, we propose a multi-stage evolution of the East Gondwana subduction zone prior to the onset of seafloor spreading between southern Zealandia and West Antarctica, as follows: The 110–100 Ma subduction of the buoyant Hikurangi Plateau decreased convergence velocities and triggered flattening of the Phoenix Plate slab. Together with the proposed rotation of the East Gondwana margin, this eventually led to extension initiation on the Chatham Rise. Synchronously, STEP faults both east and west of the Hikurangi Plateau became active. After cessation of subduction activity, slab rollback intensified extension in the Bounty Trough area. At 90 Ma, detachment of large proportions of the Phoenix Plate slab created a pathway for upwelling mantle.

A global-scale plate reorganization event is suggested to have affected all major plates between 105 to 100 Ma. We propose that cessation of subduction and fragmentation of the Phoenix Plate in response to the Hikurangi Plateau subduction significantly contributed and prolonged this event. This study highlights the effects that the subduction of an oceanic plateau can have on regional and global plate tectonics.

Data Availability Statement

The new wide-angle seismic refraction and MSC reflection data used for this publication are available upon request at Alfred Wegener Institute Helmholtz Centre for Polar and Marine Research in Bremerhaven, Germany. Maps and figures for this manuscript were created with Generic Mapping Tools (Wessel & Smith, 1998). The authors would also like to thank Emerson E&P Software, Emerson Automation Solutions, for providing licenses for the seismic software Paradigm in the scope of the Emerson Academic Program. The MCS reflection and refraction seismic data are available in the PANGAEA database hosted by the Alfred Wegener Institute, Helmholtz Centre for Polar and Marine Research in Bremerhaven (https://doi.pangaea.de/10.1594/PANGAEA.915607, https://doi.pangaea.de/10.1594/PANGAEA.915609, and https://doi.pangaea.de/10.1594/PANGAEA.915611).

References

Austermann, J., Ben-Avraham, Z., Bird, P., Heidbach, O., Schubert, G., & Stock, J. M. (2011). Quantifying the forces needed for the rapid change of Pacific plate motion at 6Ma. *Earth and Planetary Science Letters*, *307*(3–4), 289–297. https://doi.org/10.1016/j.epsl.2011.04.043

Barker, D. H. N., Sutherland, R., Henrys, S., & Bannister, S. (2009). Geometry of the Hikurangi subduction thrust and upper plate, North Island, New Zealand. *Geochemistry, Geophysics, Geosystems*, *10*, Q02007. https://doi.org/10.1029/2008GC002153

Barrett, R. S., Davy, B., Stern, T., & Gohl, K. (2018). The strike-slip west wishbone ridge and the eastern margin of the Hikurangi Plateau. *Geochemistry, Geophysics, Geosystems*, *19*, 1–18. https://doi.org/10.1002/2017GC007372

Barrier, A., Nicol, A., Browne, G. H., & Bassett, K. N. (2020). Late Cretaceous coeval multi-directional extension in south Zealandia: Implications for eastern Gondwana breakup. *Marine and Petroleum Geology*, *118*, 104383. https://doi.org/10.1016/j.marpetgeo.2020.104383

Barton, P. J. (1986). The relationship between seismic velocity and density in the continental crust—A useful constraint? *Geophysical Journal International*, *87*(1), 195–208. https://doi.org/10.1111/j.1365-246X.1986.tb04553.x

Baumann, C., Gerya, T. V., & Connolly, J. A. D. (2010). Numerical modelling of spontaneous slab breakoff dynamics during continental collision. *Geological Society Special Publication*, *332*(1), 99–114. https://doi.org/10.1144/SP332.7

Bishop, B. T., Beck, S. L., Zandt, G., Wagner, L., Long, M., Antonijevic, S. K., et al. (2017). Causes and consequences of flat-slab subduction in southern Peru. *Geosphere*, *13*(5), 1392–1407. https://doi.org/10.1130/GES01440.1

Bland, K. J., Uruski, C. I., & Isaac, M. J. (2015). Pegasus Basin, eastern New Zealand: A stratigraphic record of subsidence and subduction, ancient and modern. *New Zealand Journal of Geology and Geophysics*, *58*(4), 319–343. https://doi.org/10.1080/00288306.2015.1076862

Bradshaw, J. D. (1989). Cretaceous geotectonic patterns in the New Zealand region. *Tectonics*, *8*(4), 803–820. https://doi.org/10.1029/TC008i004p00803

Campbell, H. J., Andrews, P. B., Beu, A. G., Maxwell, P. A., Edwards, A. R., Laird, M. G., et al. (1993). *Cretaceous-Cenozoic geology and biostratigraphy of the Chatham Islands, New Zealand* (Vol. 2). Lower Hutt: Institute of Geological & Nuclear Sciences, Institute of Geological & Nuclear Sciences monograph.

Christensen, N. I., & Mooney, W. D. (1995). Seismic velocity structure and composition of the continental crust: A global view. *Journal of Geophysical Research (1978–2012)*, *100*(B6), 9761–9788. https://doi.org/10.1029/95JB00259

Cloos, M. (1993). Lithospheric buoyancy and collisional orogenesis: Subduction of oceanic plateaus, continental margins, island arcs, spreading ridges, and seamounts. *Geological Society of America Bulletin*, *105*(6), 715. https://doi.org/10.1130/0016-7606(1993)105%3C0715:LBACOS%3E2.3.CO;2

Davy, B. (2014). Rotation and offset of the Gondwana convergent margin in the New Zealand region following cretaceous jamming of Hikurangi Plateau large igneous province subduction. *Tectonics*, *33*(8), 1577–1595. https://doi.org/10.1002/2014TC003629

Davy, B., Hoernle, K., & Werner, R. (2008). Hikurangi Plateau: Crustal structure, rifted formation, and Gondwana subduction history. *Geochemistry, Geophysics, Geosystems*, *9*, Q07004. https://doi.org/10.1029/2007GC001855

Dewey, J. F. J. F., & Burke, K. (1974). Hot spots and continental break-up: Implications for collisional orogeny. *Geology*, *2*(2), 57–60. https://doi.org/10.1130/0091-7613(1974)2%3C57:HSACBI%3E2.0.CO;2

Dickinson, W. R. (1973). Widths of modern arc-trench gaps proportional to past duration of igneous activity in associated magmatic arcs. *Journal of Geophysical Research*, *78*(17), 3376–3389. https://doi.org/10.1029/jb078i017p03376

Downey, N. J., Stock, J. M., Clayton, R. W., & Cande, S. C. (2007). History of the Cretaceous Osbourn spreading center. *Journal of Geophysical Research: Solid Earth*, *112*, B04102. https://doi.org/10.1029/2006JB004550

Duesterhoeft, E., Quinteros, J., Oberhänsli, R., Bousquet, R., & de Capitani, C. (2014). Relative impact of mantle densification and eclogitization of slabs on subduction dynamics: A numerical thermodynamic/thermokinematic investigation of metamorphic density evolution. *Tectonophysics*, *637*, 20–29. https://doi.org/10.1016/j.tecto.2014.09.009

Duretz, T., Gerya, T. V., & May, D. a. (2011). Numerical modelling of spontaneous slab breakoff and subsequent topographic response. *Tectonophysics*, *502*(1–2), 244–256. https://doi.org/10.1016/j.tecto.2010.05.024

Eagles, G., Gohl, K., & Larter, R. D. (2004). High-resolution animated tectonic reconstruction of the South Pacific and West Antarctic Margin. *Geochemistry, Geophysics, Geosystems*, *5*, Q07004. https://doi.org/10.1029/2003GC000657

Edwards, S. J., Schellart, W. P., & Duarte, J. C. (2015). Geodynamic models of continental subduction and obduction of overriding plate forearc oceanic lithosphere on top of continental crust. *Tectonics*, *34*, 1494–1515. https://doi.org/10.1002/2015TC003884

Espurt, N., Funiciello, F., Martinod, J., Guillaume, B., Regard, V., & Faccenna, C. (2008). Flat subduction dynamics and deformation of the South American plate: Insights from analog modeling. *Tectonics*, *27*, 1–19. https://doi.org/10.1029/2007TC002175

Fromm, T. (2016). PRay—A graphical user interface for interactive visualization and modification of rayinvr models. *Journal of Applied Geophysics*, *124*, 1–3. https://doi.org/10.1016/j.jappgeo.2015.11.004

Furumoto, A. S., Webb, J. P., Odegard, M. E., & Hussong, D. M. (1976). Seismic studies on the Ontong Java Plateau, 1970. *Tectonophysics*, *34*(1–2), 71–90. https://doi.org/10.1016/0040-1951(76)90177-3

Gerya, T. V., Yuen, D. A., & Maresch, W. V. (2004). Thermomechanical modelling of slab detachment. *Earth and Planetary Science Letters*, *226*(1–2), 101–116. https://doi.org/10.1016/j.epsl.2004.07.022

Gianni, G. M., García, H. P. A., Lupari, M., Pesce, A., & Folguera, A. (2017). Plume overriding triggers shallow subduction and orogeny in the southern central Andes. *Gondwana Research*, *49*, 387–395. https://doi.org/10.1016/j.gr.2017.06.011

Godfrey, N. J., Davey, F., Stern, T. A., & Okaya, D. (2001). Crustal structure and thermal anomalies of the Dunedin region, South Island, New Zealand. *Journal of Geophysical Research*, *106*(B12), 30,835–30,848. https://doi.org/10.1029/2000JB000006

Gohl, K., & Werner, R. (2016). The expedition SO246 of the research vessel SONNE to the Chatham Rise in 2016. In *Berichte zur polar- und Meeresforschung = Reports on polar and marine research*. Bremerhaven, Germany: Alfred Wegener Institute for Polar and Marine Research. https://doi.org/10.2312/BzPM_0698_2016

Govers, R., & Wortel, M. J. R. (2005). Lithosphere tearing at STEP faults: Response to edges of subduction zones. *Earth and Planetary Science Letters*, *236*(1–2), 505–523. https://doi.org/10.1016/j.epsl.2005.03.022

Grobys, J. W. G., Gohl, K., Davy, B., Uenzelmann-Neben, G., Deen, T., & Barker, D. (2007). Is the bounty trough off eastern New Zealand an aborted rift? *Journal of Geophysical Research*, *112*, B03103. https://doi.org/10.1029/2005JB004229

Grobys, J. W. G., Gohl, K., Uenzelmann-Neben, G., Davy, B., & Barker, D. (2009). Extensional and magmatic nature of the Campbell plateau and great South Basin from deep crustal studies. *Tectonophysics*, *472*(1–4), 213–225. https://doi.org/10.1016/j.tecto.2008.05.003

Henrys, S., Wech, A., Sutherland, R., Stern, T., Savage, M., Sato, H., et al. (2013). SAHKE geophysical transect reveals crustal and subduction zone structure at the southern Hikurangi margin, New Zealand. *Geochemistry, Geophysics, Geosystems*, *14*, 2063–2083. https://doi.org/10.1002/ggge.20136

Herath, P., Stern, T. A., Savage, M. K., Bassett, D., Henrys, S., & Boulton, C. (2020). Hydration of the crust and upper mantle of the Hikurangi Plateau as it subducts at the southern Hikurangi margin. *Earth and Planetary Science Letters*, *541*, 116271. https://doi.org/10.1016/j.epsl.2020.116271

Hochmuth, K., & Gohl, K. (2017). Collision of Manihiki plateau fragments to accretional margins of northern Andes and Antarctic peninsula. *Tectonics*, *36*, 229–240. https://doi.org/10.1002/2016TC004333

Hochmuth, K., Gohl, K., & Uenzelmann-Neben, G. (2015). Playing jigsaw with Large Igneous Provinces—A plate tectonic reconstruction of Ontong Java Nui,West Pacific. *Geochemistry, Geophysics, Geosystems*, *16*, 3789–3807. https://doi.org/10.1002/2015GC006036

Hochmuth, K., Gohl, K., Uenzelmann-Neben, G., & Werner, R. (2019). Multiphase magmatic and tectonic evolution of a large igneous province—Evidence from the crustal structure of the Manihiki plateau, western Pacific. *Tectonophysics*, *750*, 434–457. https://doi.org/10.1016/j.tecto.2018.11.014

Hoernle, K., Hauff, F., van den Bogaard, P., Werner, R., Mortimer, N., Geldmacher, J., et al. (2010). Age and geochemistry of volcanic rocks from the Hikurangi and Manihiki oceanic plateaus. *Geochimica et Cosmochimica Acta*, *74*(24), 7196–7219. https://doi.org/10.1016/j.gca.2010.09.030

Hoernle, K., Timm, C., Hauff, F., Tappenden, V., Werner, R., Jolis, E. M., et al. (2020). Late cretaceous (99–69 Ma) basaltic intraplate volcanism on and around Zealandia: Tracing upper mantle geodynamics from Hikurangi Plateau collision to Gondwana breakup and beyond. *Earth and Planetary Science Letters*, *529*, 115864. https://doi.org/10.1016/j.epsl.2019.115864

Homrighausen, S., Hoernle, K., Geldmacher, J., Wartho, J. A., Hauff, F., Portnyagin, M., et al. (2018). Unexpected HIMU-type late-stage volcanism on the Walvis ridge. *Earth and Planetary Science Letters*, *492*, 251–263. https://doi.org/10.1016/j.epsl.2018.03.049

Huangfu, P., Wang, Y., Li, Z., Fan, W., & Zhang, Y. (2016). Effects of crustal eclogitization on plate subduction/collision dynamics: Implications for India-Asia collision. *Journal of Earth Science*, *27*(5), 727–739. https://doi.org/10.1007/s12583-016-0701-9

Jacob, J.-B., Scott, J. M., Turnbull, R. E., Tarling, M. S., & Sagar, M. W. (2017). High- to ultrahigh-temperature metamorphism in the lower crust: An example resulting from Hikurangi Plateau collision and slab rollback in New Zealand. *Journal of Metamorphic Geology*, *35*(8), 831–853. https://doi.org/10.1111/jmg.12257

Knesel, K. M., Cohen, B. E., Vasconcelos, P. M., & Thiede, D. S. (2008). Rapid change in drift of the Australian plate records collision with Ontong Java plateau. *Nature*, *454*(7205), 754–757. https://doi.org/10.1038/nature07138

Laird, M. G., & Bradshaw, J. D. (2004). The break-up of a long-term relationship: The Cretaceous separation of New Zealand from Gondwana. *Gondwana Research*, *7*(1), 273–286. https://doi.org/10.1016/S1342-937X(05)70325-7

Larter, R. D., Cunningham, A. P., Barker, P. F., Gohl, K., & Nitsche, O. (2002). Tectonic evolution of the Pacific margin of Antarctica 1. Late Cretaceous tectonic reconstructions. *Journal of Geophysical Research*, *107*(B12), 2345. https://doi.org/10.1029/2000JB000052

Li, Z. H., Xu, Z., Gerya, T., & Burg, J. P. (2013). Collision of continental corner from 3-D numerical modeling. *Earth and Planetary Science Letters*, *380*, 98–111. https://doi.org/10.1016/j.epsl.2013.08.034

Liu, L., Gurnis, M., Seton, M., Saleeby, J., Müller, R. D., & Jackson, J. M. (2010). The role of oceanic plateau subduction in the Laramide orogeny. *Nature Geoscience*, *3*(5), 353–357. https://doi.org/10.1038/ngeo829

Luyendyk, B. P., Sorlien, C. C., Wilson, D. S., Bartek, L. R., & Siddoway, C. S. (2001). Structural and tectonic evolution of the Ross Sea rift in the Cape Colbeck region, Eastern Ross Sea, Antarctica. *Tectonics*, *20*(6), 933–958. https://doi.org/10.1029/2000tc001260

Magni, V., Allen, M. B., van Hunen, J., & Bouilhol, P. (2017). Continental underplating after slab break-off. *Earth and Planetary Science Letters*, *474*, 59–67. https://doi.org/10.1016/j.epsl.2017.06.017

Mann, P., & Taira, A. (2004). Global tectonic significance of the Solomon Islands and Ontong Java Plateau convergent zone. *Tectonophysics*, *389*(3-4 SPEC.ISS), 137–190. https://doi.org/10.1016/j.tecto.2003.10.024

Matthews, K. J., Maloney, K. T., Zahirovic, S., Williams, S. E., Seton, M., & Müller, R. D. (2016). Global plate boundary evolution and kinematics since the late Paleozoic. *Global and Planetary Change*, *146*, 226–250. https://doi.org/10.1016/j.gloplacha.2016.10.002

Matthews, K. J., Seton, M., & Müller, R. D. (2012). A global-scale plate reorganization event at 105-100 Ma. *Earth and Planetary Science Letters*, *355-356*, 283–298. https://doi.org/10.1016/j.epsl.2012.08.023

McCoy-West, A. J., Baker, J. A., Faure, K., & Wysoczanski, R. (2010). Petrogenesis and origins of mid-cretaceous continental intraplate volcanism in Marlborough, New Zealand: Implications for the long-lived HIMU magmatic mega-province of the SW Pacific. *Journal of Petrology*, *51*(10), 2003–2045. https://doi.org/10.1093/petrology/egq046

Mochizuki, K., Sutherland, R., Henrys, S., Bassett, D., Van Avendonk, H., Arai, R., et al. (2019). Recycling of depleted continental mantle by subduction and plumes at the Hikurangi Plateau large igneous province, southwestern Pacific Ocean. *Geology*, *47*(8), 795–798. https://doi.org/10.1130/G46250.1

Mortimer, N., Campbell, H. J., & Moerhuis, N. (2019). Chatham schist. *New Zealand Journal of Geology and Geophysics*, *63*(2), 237–249. https://doi.org/10.1080/00288306.2019.1662817

Mortimer, N., Davey, F. J., Melhuish, A., Yu, J., & Godfrey, N. J. (2002). Geological interpretation of a deep seismic reflection profile across the Eastern Province and Median Batholith, New Zealand: Crustal architecture of an extended Phanerozoic convergent orogen. *New Zealand Journal of Geology and Geophysics*, *45*(3), 349–363. https://doi.org/10.1080/00288306.2002.9514978

Mortimer, N., Hoernle, K., Hauff, F., Palin, J. M., Dunlap, W. J., Werner, R., & Faure, K. (2006). New constraints on the age and evolution of the Wishbone Ridge, southwest Pacific cretaceous microplates, and Zealandia - West Antarctica breakup. *Geology*, *34*(3), 185–188. https://doi.org/10.1130/G22168.1

Mortimer, N., Kohn, B., Seward, D., Spell, T., & Tulloch, A. (2016). Reconnaissance thermochronology of southern Zealandia. *Journal of the Geological Society*, *173*(2), 370–383. https://doi.org/10.1144/jgs2015-021

Mortimer, N., van den Bogaard, P., Hoernle, K., Timm, C., Gans, P. B., Werner, R., & Riefstahl, F. (2019). Late cretaceous oceanic plate reorganization and the breakup of Zealandia and Gondwana. *Gondwana Research*, *65*, 31–42. https://doi.org/10.1016/j.gr.2018.07.010

Olierook, H. K. H., Jourdan, F., Whittaker, J. M., Merle, R. E., Jiang, Q., Pourteau, A., & Doucet, L. S. (2020). Timing and causes of the mid-Cretaceous global plate reorganization event. *Earth and Planetary Science Letters*, *534*, 116071. https://doi.org/10.1016/j.epsl.2020.116071

Panter, K. S., Blusztajn, J., Hart, S. R., Kyle, P. R., Esser, R., & McIntosh, W. C. (2006). The origin of HIMU in the SW Pacific: Evidence from intraplate volcanism in Southern New Zealand and Subantarctic Islands. *Journal of Petrology*, *47*(9), 1673–1704. https://doi.org/10.1093/petrology/egl024

Reyners, M. (2013). The central role of the Hikurangi Plateau in the Cenozoic tectonics of New Zealand and the Southwest Pacific. *Earth and Planetary Science Letters*, *361*, 460–468. https://doi.org/10.1016/j.epsl.2012.11.010

Reyners, M., Eberhart-Phillips, D., & Bannister, S. (2011). Tracking repeated subduction of the Hikurangi Plateau beneath New Zealand. *Earth and Planetary Science Letters*, *311*(1–2), 165–171. https://doi.org/10.1016/j.epsl.2011.09.011

Reyners, M., Eberhart-Phillips, D., Upton, P., & Gubbins, D. (2017). Three-dimensional imaging of impact of a large igneous province with a subduction zone. *Earth and Planetary Science Letters*, *460*, 143–151. https://doi.org/10.1016/j.epsl.2016.12.025

Riefstahl, F., Gohl, K., Davy, B., Mortimer, N., Hoernle, K., Timm, C., et al. (2020). Cretaceous intracontinental rifting at the southern Chatham Rise margin and initialisation of seafloor spreading between Zealandia and Antarctica. *Tectonophysics*, *776*, 228298. https://doi.org/10.1016/j.tecto.2019.228298

Schellart, W. P., Freeman, J., Stegman, D. R., Moresi, L., & May, D. (2007). Evolution and diversity of subduction zones controlled by slab width. *Nature*, *446*(7133), 308–311. https://doi.org/10.1038/nature05615

Scherwath, M., Kopp, H., Flueh, E. R., Henrys, S. A., Sutherland, R., Stagpoole, V. M., et al. (2010). Fore-arc deformation and under-plating at the northern Hikurangi margin, New Zealand. *Journal of Geophysical Research*, *115*, B06408. https://doi.org/10.1029/2009JB006645

Scherwath, M., Stern, T., Davey, F., Okaya, D., Holbrook, W. S., Davies, R., & Kleffmann, S. (2003). Lithospheric structure across oblique continental collision in New Zealand from wide-angle P wave modeling. *Journal of Geophysical Research*, *108*(B12), 2566. https://doi.org/10.1029/2002JB002286

Schlindwein, V., & Jokat, W. (1999). Structure and evolution of the continental crust of northern east Greenland from integrated geo-physical studies. *Journal of Geophysical Research*, *104*(B7), 15,227–15,245. https://doi.org/10.1029/1999JB900101

Schmidt, S., Götze, H., Fichler, C., Ebbing, J., & Alvers, M. R. (2007). 3D Gravity, FTG and magnetic modeling: the new IGMAS+ software. In *EGM 2007 International Workshop* (pp. 1–4). Capri: European Association of Geoscientists and Engineers.

Schwartz, J. J., Stowell, H. H., Klepeis, K. A., Tulloch, A. J., Kylander-Clark, A. R. C., Hacker, B. R., & Coble, M. A. (2016). Thermochronology of extensional orogenic collapse in the deep crust of Zealandia. *Geosphere*, *12*(3), 647–677. https://doi.org/10.1130/GES01232.1

Seton, M., Müller R. D., Zahirovic S., Gaina C., Torsvik T., Shephard G., et al. (2012). Global continental and ocean basin reconstructions since 200Ma. *Earth-Science Reviews*, *113*(3-4), 212–270. https://doi.org/10.1016/j.earscirev.2012.03.002

Smith, E. G. C., Stern, T., & O' Brien, B. (1995). A seismic velocity profile across the central South Island, New Zealand, from explosion data. *New Zealand Journal of Geology and Geophysics*, *38*(4), 565–570. https://doi.org/10.1080/00288306.1995.9514684

Stern, T., Lamb, S., Moore, J. D. P., Okaya, D., & Hochmuth, K. (2020). High mantle seismic P-wave speeds as a signature for gravitational spreading of superplumes. *Science Advances*, *6*(22), eaba7118. https://doi.org/10.1126/sciadv.aba7118

Strogen, D. P., Seebeck, H., Nicol, A., & King, P. R. (2017). Two-phase Cretaceous–Paleocene rifting in the Taranaki Basin region, New Zealand; implications for Gondwana break-up. *Journal of the Geological Society*, *174*(5), 929–946. https://doi.org/10.1144/jgs2016-160

Taira, A., Mann, P., & Rahardiawan, R. (2004). Incipient subduction of the Ontong Java Plateau along the North Solomon trench. *Tectonophysics*, *389*(3-4 SPEC.ISS), 247–266. https://doi.org/10.1016/j.tecto.2004.07.052

Taylor, B. (2006). The single largest oceanic plateau: Ontong Java-Manihiki-Hikurangi. *Earth and Planetary Science Letters*, *241*(3–4), 372–380. https://doi.org/10.1016/j.epsl.2005.11.049

Timm, C., Davy, B., Haase, K., Hoernle, K. A., Graham, I. J., de Ronde, C. E. J., et al. (2014). Subduction of the oceanic Hikurangi Plateau and its impact on the Kermadec arc. *Nature Communications*, *5*(1), 4923. https://doi.org/10.1038/ncomms5923

Timm, C., Leybourne, M. I., Hoernle, K., Wysoczanski, R. J., Hauff, F., Handler, M., et al. (2016). Trench-perpendicular geochemical variation between two adjacent Kermadec arc volcanoes rumble II east and west: The role of the subducted Hikurangi Plateau in ele-ment recycling in arc magmas. *Journal of Petrology*, *57*(7), 1335–1360. https://doi.org/10.1093/petrology/egw042

Tozer, B., Stern, T. A., Lamb, S. L., & Henrys, S. A. (2017). Crust and upper-mantle structure of Wanganui Basin and southern Hikurangi margin, North Island, New Zealand as revealed by active source seismic data. *Geophysical Journal International*, *211*(2), 718–740. https://doi.org/10.1093/gji/ggx303

Tulloch, A. J., & Kimbrough, D. L. (2003). Paired plutonic belts in convergent margins and the development of high Sr/Y magmatism: Peninsular ranges batholith of Baja-California and median batholith of New Zealand. *Special Paper of the Geological Society of America*, *374*(303), 275–295. https://doi.org/10.1130/0-8137-2374-4.275

Tulloch, A. J., Mortimer, N., Ireland, T. R., Waight, T. E., Maas, R., Palin, M., et al. (2019). Reconnaissance basement geology and tectonics of south Zealandia. *Tectonics*, *38*(2), 516–551. https://doi.org/10.1029/2018TC005116

Van Avendonk, H. J. A., Holbrook, W. S., Okaya, D., Austin, J. K., Davey, F., & Stern, T. (2004). Continental crust under compression: A seismic refraction study of South Island Geophysical Transect I, South Island, New Zealand. *Journal of Geophysical Research*, *109*, B06302. https://doi.org/10.1029/2003JB002790

van der Meer, Q. H. A., Storey, M., Scott, J. M., & Waight, T. E. (2016). Abrupt spatial and geochemical changes in lamprophyre magmatism related to Gondwana fragmentation prior, during and after opening of the Tasman Sea. *Gondwana Research*, *36*, 142–156. https://doi.org/10.1016/j.gr.2016.04.004

van der Meer, Q. H. A., Waight, T. E., Whitehouse, M. J., & Andersen, T. (2017). Age and petrogenetic constraints on the lower glassy ignimbrite of the Mount Somers volcanic group, New Zealand. *New Zealand Journal of Geology and Geophysics*, *60*(3), 209–219. https://doi.org/10.1080/00288306.2017.1307232

van Hunen, J., & Allen, M. B. (2011). Continental collision and slab break-off: A comparison of 3-D numerical models with observations. *Earth and Planetary Science Letters*, *302*(1–2), 27–37. https://doi.org/10.1016/j.epsl.2010.11.035

van Hunen, J., van den Berg, A. P., & Vlaar, N. J. (2002). On the role of subducting oceanic plateaus in the development of shallow flat subduction. *Tectonophysics*, *352*(3–4), 317–333. https://doi.org/10.1016/S0040-1951(02)00263-9

Wessel, P., & Smith, W. H. F. (1998). New, improved version of generic mapping tools released. *Eos, Transactions of the American Geophysical Union*, *79*(47), 579. https://doi.org/10.1029/98EO00426

Wobbe, F., Gohl, K., Chambord, A., & Sutherland, R. (2012). Structure and breakup history of the rifted margin of West Antarctica in relation to Cretaceous separation from Zealandia and Bellingshausen plate motion. *Geochemistry, Geophysics, Geosystems*, *13*(4), 1–19. https://doi.org/10.1029/2011GC003742

Wood, R. A., & Anderson, H. J. (1989). Basement structure at the Chatham Islands. *Journal of the Royal Society of New Zealand*, *19*(3), 269–282. https://doi.org/10.1080/03036758.1989.10427182

Wood, R. A., Andrews, P. B., & Herzer, R. H. (1989). *Cretaceous and Cenozoic geology of the Chatham Rise Region, South Island, New Zealand (New Zealand)*. Lower Hutt, New Zealand: New Zealand Geological Survey.

Wortel, M. J. R., & Spakman, W. (2000). Subduction and slab detachment in the Mediterranean-Carpathian region. *Science*, *290*(5498), 1910–1917. https://doi.org/10.1126/science.290.5498.1910

Zelt, B. C. (2004). *ZP—Software for plotting & picking seismic refraction data in SEGY format. Hawaii Institute of Geophysics and Planetology, School of Ocean and Earth Science and Technology*. Honolulu: University of Hawaii.

Zelt, C. A., & Smith, R. B. (1992). Seismic traveltime inversion for 2-D crustal velocity structure. *Geophysical Journal International*, *108*(1), 16–34. https://doi.org/10.1111/j.1365-246X.1992.tb00836.x

Zhang, G.-L., & Li, C. (2016). Interactions of the Greater Ontong Java mantle plume component with the Osbourn Trough. *Scientific Reports*, *6*(1), 37561. https://doi.org/10.1038/srep37561